# Effects of Composition and Ausaging on Microstructure and Magnetic Shape Memory Response of Fe-Ni-Co-Ti Alloys

by

**Ryoji Hayashi**
B.E., Materials Science and Engineering (1991)
Osaka University

Submitted to the Department of Materials Science and Engineering
in Partial Fulfillment of the Requirements for the degree of
**Master of Science in Materials Science and Engineering**

at the
**Massachusetts Institute of Technology**
June 1998



Signature of Author_____
Department of Materials Science and Engineering
May 8, 1998

Certified by_____
Samuel M. Allen
Professor of Physical Metallurgy
Thesis Supervisor

Certified by_____
Robert C. O'Handley
Senior Research Scientist
Thesis Co-Advisor

Accepted by_____
Linn W. Hobbs
John F. Elliott Professor of Materials
Chairman, Departmental Committee on Graduate Students



Science

# Effects of Composition and Ausaging on Microstructure and Magnetic Shape Memory Response of Fe-Ni-Co-Ti Alloys

by

**Ryoji Hayashi**

Submitted to the Department of Materials Science and Engineering
On May 8, 1998 in partial fulfillment of the
requirements for the Degree of Master of Science in
Materials Science and Engineering

## ABSTRACT

Magnetic Shape-Memory (MSM) materials are a new category of actuator materials with the potential to produce both large actuator strain and rapid response. To explore the possibility of developing MSM materials based on Fe-Ni-Co-Ti alloys, the effects of chemical composition (Co/Ni ratio) and ausaging on microstructure and magnetic shape-memory response were studied. A suitable choice of chemical composition and ausaging enabled the formation of martensite at or above room temperature. Most of the observed martensite morphology was lenticular or a mixture of lenticular and thin-plate. A specimen with the lowest martensite start temperature (203 K) exhibited a typical thin-plate morphology, which is fully twinned and believed to be required for MSM materials.

Ausaging treatments were effective in increasing hardness likely through the precipitation of $(Fe,Ni,Co)_3Ti$, and higher Co/Ni ratios accelerated the aging kinetics. Ausaging also increased the saturation magnetization ($M_s$) through a structural change from austenite to martensite, though the $M_s$ of martensite was relatively insensitive to the aging conditions. From these results, it can be expected that Fe-Ni-Co-Ti has the potential to show the same order of strains to $Ni_2MnGa$ if the magnitude of transformation strain is the same.

An Fe-Ni-Co-Ti specimen with thin-plate martensite exhibited a significant conventional shape-memory effect. However, no significant magnetic field-induced strains were observed, even in a specimen with thin-plate martensite, and this result is thought to be due to the random grain orientation in the polycrystalline materials studied.

| | |
|---|---|
| Thesis Supervisor: | Samuel M. Allen |
| Title: | Professor of Physical Metallurgy |
| Thesis Co-Advisor: | Robert C. O'Handley |
| Title: | Senior Research Scientist |

# Table of Content

# List of Figures

# List of Tables

## Acknowledgements

I have greatly appreciated the support and advice of Professor Samuel M. Allen through out research. His wide knowledge and encouragement always helped me overcome challenges.

I have also appreciated the invaluable guidance, helpful discussion, and innovative ideas of Dr. Robert C. O'Handley.

I am greatly indebted to all of my colleagues in Prof. Allen's group and Dr. O'Handley's group, especially to Steve Murray, Miguel Marioni, Matt Farinelli, Katherine Oates, and Jiankang Huang. I enjoyed doing research in MSM materials for five months with all of you.

I would like to thank Ms. Yin-Lin Xie, Mr. Pat Kearney, and Mr. Toby Bashaw for help on my experiments, and Ms. Rachel Kemper and Mr. Robin Lippincott for their assistance through my research.

I am also grateful to Sanyo Special Steel Co., Ltd. for their generosity in giving me the opportunity and financial support to study in the United State for two years. I would like to express my particular gratitude to Dr. Hisashi Matsunaga, Mr. Toshio Sato, Mr. Koji Kishimoto, and Mr. Yasushi Haruna for their support of my stay in MIT.

Finally, I would like to thank to my parents for their great love and encouragement for my time in the United States.

# 1 Introduction

Actuator materials are defined as substances which transfer electro-magnetic energy or thermal energy to mechanical energy. One of their applications is active vibration control in automobiles and airplanes. To be used widely in the engineering world, actuator materials must fulfill several requirements. They must show large stroke and force with rapid response and high toughness. They also must be operated at or above room temperature and produced economically in large quantities.

The most important actuator materials are piezoelectric, magnetostrictive, and shape-memory materials [1]. Piezoelectric and magnetostrictive materials generate strains through the application of electrical and magnetic fields, respectively. Piezoelectric materials have good high-frequency response, but only generate small strains and are brittle. Magnetostrictive Fe-Dy-Tb intermetallics (e.g., Terfenol) produce strains up to 0.24 %, about two to three times higher stress (around 100 MPa) than piezoelectric materials, and respond up to several kHz. Therefore, magnetostrictive materials have been applied to active vibration control and precision tooling. Shape-memory materials generate large actuation strains and forces by a change of crystal structure, but their frequency response is limited because the strains are generated by changing the temperature of the actuator material.

Magnetic shape-memory (MSM) materials are a new category of actuator materials with the potential to produce both the large actuator strain of shape-memory materials and the rapid response of magnetostrictive materials [1,2,3]. Actuation of MSM

materials is based on the magnetic-field control of the martensite structure in shape-memory alloys. The mechanisms of shape changes of actuator materials are shown in Figure 1-1. Magnetostrictive materials change their shape by rotation of the domain magnetization in the material. The magnetization vector $\boldsymbol{M}$ becomes parallel to the applied magnetic field $\boldsymbol{H}$ in the unit cell, which results in the elongation of the unit cell (Figure 1-1(a)). Shape-memory materials deform by applied shear stress through the reorientation of unit cells in twinned martensite (Figure 1-1(b)). Applied stress can rotate a twin variant into an orientation which accommodates applied stress [4]. Other twin variants are converted into this preferred orientation through twin boundary motions that result in a shape change of the material.

In the case of MSM materials the mechanism of shape change is thought to be due to the reorientation of martensite unit cells induced by an applied magnetic field (Figure 1-1(c))[1]. In crystalline ferromagnetic materials, magnetization vectors tend to lie along specific crystallographic axes called directions of easy magnetization. The magnetocrystalline anisotropy energy describes the tendency for the magnetization to lie along these directions in the absence of an external field. When an external magnetic field is applied, the magnetization tends to turn from the easy direction of the unit cell to the direction of external magnetic field if the field energy, $M_sH$, is greater than the anisotropy energy (see magnetostrictive materials in Figure 1-1(a)). If the anisotropy energy is high, a large magnetic field is required to turn the magnetization. If the energy of the twin boundary motion is smaller than anisotropy energy, then the magnetic field produces twin boundary motions, thus lowering the Zeeman energy, $M_sH$, without rotating $M_s$ from its easy direction in the unit cell. The rotation of a unit cell by the applied magnetic field is

shown in Figure 1-1(c). Magnetization then remains in the original easy direction in the rotated unit cells. This rotation of unit cells results in the growth of unit cells with preferred orientations and causes a shape change of the material as in shape-memory materials (Figure 1-2). The criterion of the rotation of unit cells by magnetic field is expressed as [1]:

$$U_k > E_t + W + E_0$$

where $U_k$ is the anisotropy energy, $E_t$ is the energy of twin boundary motions, $W$ is the work done by the actuator material (if the rotation is assisted by external stress, $W$ is negative), and $E_0$ includes internal strain and other energy terms. Therefore, the MSM effect depends on the relative magnitude of the anisotropy energy and the energy of twin boundary motions; MSM materials are required to exhibit high magnetocrystalline anisotropy energy and low energy of twin boundary motions (high twin-boundary mobility).

Because most shape-memory materials undergo thermoelastic martensitic transformation and possess mobile twin boundaries or martensite interfaces, ferromagnetic shape-memory materials are of interest as candidate MSM materials. As the reorientation of twin variants generates recoverable strains of several percent in shape-memory materials, the magnetic-field control of reorientation of twin variants of shape-memory materials can be expected to produce strains of the same order.

MSM effects of ferromagnetic shape-memory Heusler alloys $Ni_2MnGa$ [5,6,7] and Fe-Pd alloys [8] have already been reported. A magnetic field-induced strain of nearly 0.2

% was achieved in $Ni_2MnGa$ single crystals with magnetic fields of 8 kOe at 265 K in 1996 (Figure 1-3) [5]. The martensite start temperature of this alloy was 276 K.

James and Wuttig reported three notable results in 1997 [8]. Single-crystal $Fe_{70}Pd_{30}$ showed 0.5% field-induced strain with magnetic fields of 8 kOe at 256 K. This system possesses excellent magnetic properties for the MSM effect, namely large saturation magnetization (1400 emu/cm$^3$) and a magnetocrystalline anisotropy constant on the order of $10^7$-$10^8$ ergs/cm$^3$. The second result of their work is the observation of twin variant rearrangement, which supports the suggested mechanism of MSM effects. Moreover, field-induced strain of 0.1 % under a compressive stress of 5 MPa during field drive was observed with magnetic field of 2 kOe in single-crystal $Fe_{70}Pd_{30}$.

Though these two alloys present a promising future for MSM materials, there still remain some major challenges toward practical applications [7]:

1. The operating temperatures of MSM materials must be increased at or above room temperature. This requires the increase of martensite start transformation temperatures ($T_{Ms}$), which can be achieved through suitable selection of material systems with proper addition of alloying elements.
2. MSM materials must exhibit large strains against significant loads. Though the performance of MSM materials under loads is not well characterized, high hardness is believed to be helpful to fulfill this requirement.
3. High toughness and low production cost are required. Ordered intermetallics and alloys with noble or rare-earth metals, as well as single crystals are not good choices from these standpoints.

In 1998, the performance of polycrystalline materials was studied in $Ni_2MnGa$ to fulfill the above requirements [7]. Field-induced strain of up to 150 ppm at 281 K, just below $T_{Ms}$, was observed, though this was more than one order of magnitude smaller than that of single-crystal $Ni_2MnGa$ mentioned above [5]. More than 100 ppm of field-induced strain under load was also measured and it is worth noting that this strain was achieved at a temperature above $T_{Ms}$ due to stress-induced martensite. This stress-induced martensitic transformation is interesting for two reasons: stress preferentially aligns texture, and stress-induced martensite extends the applicable temperature range, as martensite is obtained at higher temperature than $T_{Ms}$.

Fe-Ni-Co-Ti alloys are also promising as MSM materials because of low material cost, high productivity, high ductility, and strong magnetization. Moreover, this system has been well studied as a conventional shape-memory alloy for two decades [9, 10, 11, 12, 13, 14, 15, 16]. Almost complete shape-memory effects have been observed with the combination of proper chemical composition, ausaging, and thermomechanical processes. The addition of 10 % Co to Fe-31Ni-3Ti, that is, Fe-31Ni-10Co-3Ti, exhibited an almost complete shape-memory effect with ausaging at 873 K [9]. Also, Fe-29Ni-18Co-3.5Ti showed a shape-memory effect with thermomechanical processes [12]. Although such shape-memory effects were achieved with $T_{Ms}$ below room temperature, the Fe-Ni-Co phase diagram (Figure 1-4) shows that some compositions exhibit martensite start temperatures and Curie temperatures above room temperature [17]. Moreover, no report has been made about the MSM effects in Fe-Ni-Co-Ti alloys.

Therefore, this research is the first to examine Fe-Ni-Co-Ti alloys as MSM materials with a large amount of field-induced strain, large actuation force, and high $T_{Ms}$.

A preliminary investigation has been carried out to assess about the effects of chemical composition and ausaging on microstructure and magnetic shape-memory response, because chemical composition and ausaging are two major factors which control conventional shape-memory effect, and they are believed to be the key parameters even on MSM behavior. Although alloy compositions of Ni from 28 % to 33 %, Co from 10 % to 18 %, and Ti around 4 % have been studied as conventional shape-memory alloys [9, 10, 11, 12, 13, 14, 15, 16], the appropriate range of chemical composition for MSM materials is unknown. In this composition range, $T_{Ms}$ can be increased by increased Co content in Fe-Ni-Co alloys (see Figure 1-4), although the effects of Ti addition on $T_{Ms}$ are unknown. Also, ausaging is thought to be the indispensable prerequisite for introducing shape-memory effect [11, 15]. Finely dispersed, ordered, and coherent γ' particles with the composition of $(Fe,Ni,Co)_3Ti$, which formed during ausaging, are thought to promote thermoelasticity through the increase of hardness [15]. Based on these earlier studies and the Fe-Ni-Co phase diagram, three ingot compositions were cast with different amounts of Ni and Co (namely higher Co/Ni ratios) and then ausaged at 873 K or 973 K for 1 h, 3 h, or 10 h, in order to examine the effects of Co/Ni ratio and ausaging on mechanical and magnetic properties. The alloy compositions selected are shown in Table 1-1 and the alloy designations S1, S2, and S3 are used in the remainder of this thesis.

**Table 1-1 Chemical compositions of each ingot (wt. %)**

| Alloy name | Fe | Ni | Co | Ti |
|---|---|---|---|---|
| S1 | 52 | 29 | 15 | 4 |
| S2 | 52 | 27 | 17 | 4 |
| S3 | 52 | 25 | 19 | 4 |

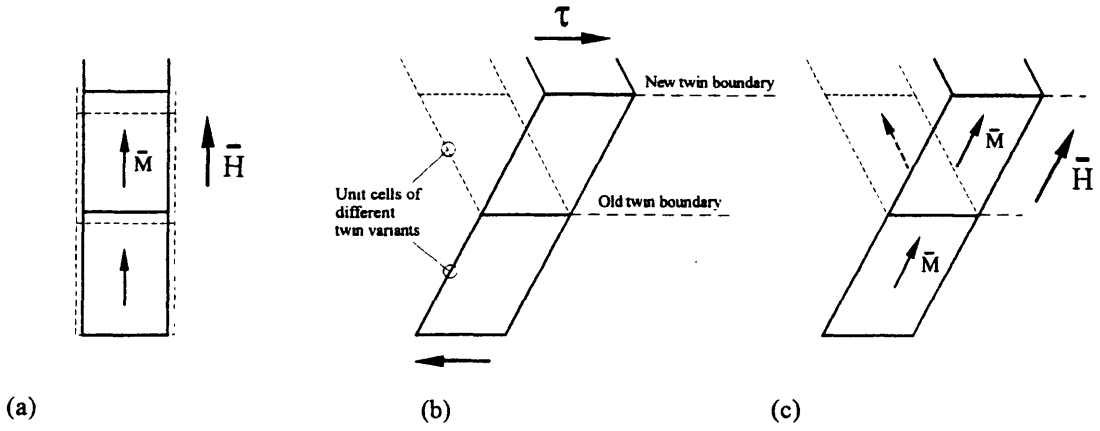


**Figure 1-1 Schematic illustration of shape change mechanisms of (a) magnetostrictive, (b) shape memory, and (c) magnetic shape memory materials [1].**

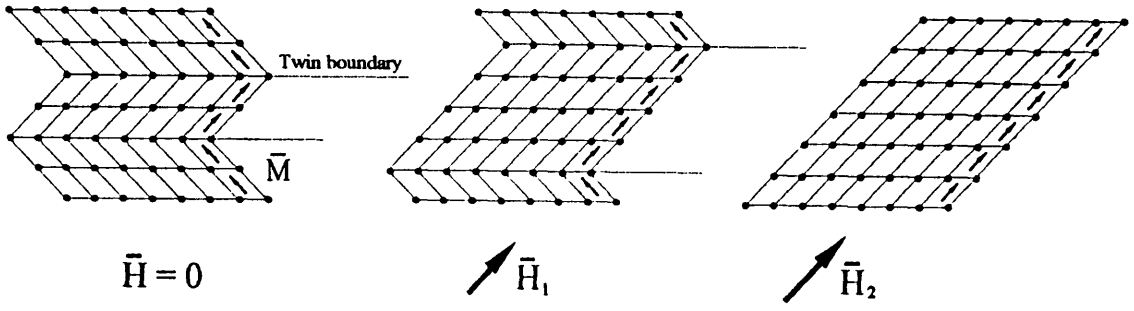


**Figure 1-2 Twin variant growth induced by the external magnetic field ($H_1 < H_2$) [6].**

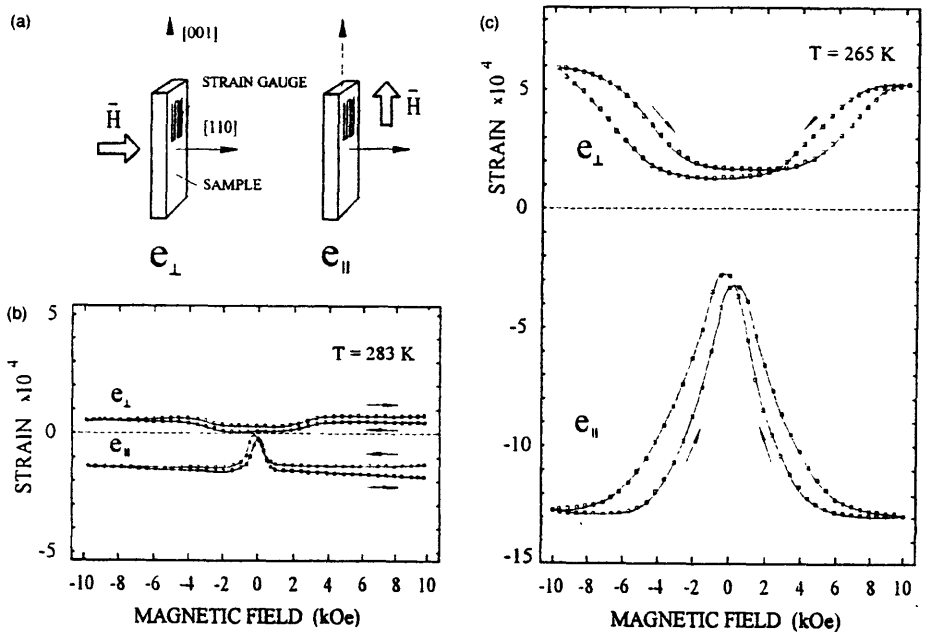


**Figure 1-3 Strains induced by the magnetic field H applied in the [110] and [001] directions in a $Ni_2MnGa$ single crystal. The strain was measured in the [001] direction. The measurements were performed at 283 K (left: austenitic phase) and at 265 K (right: martensitic phase) [5].**

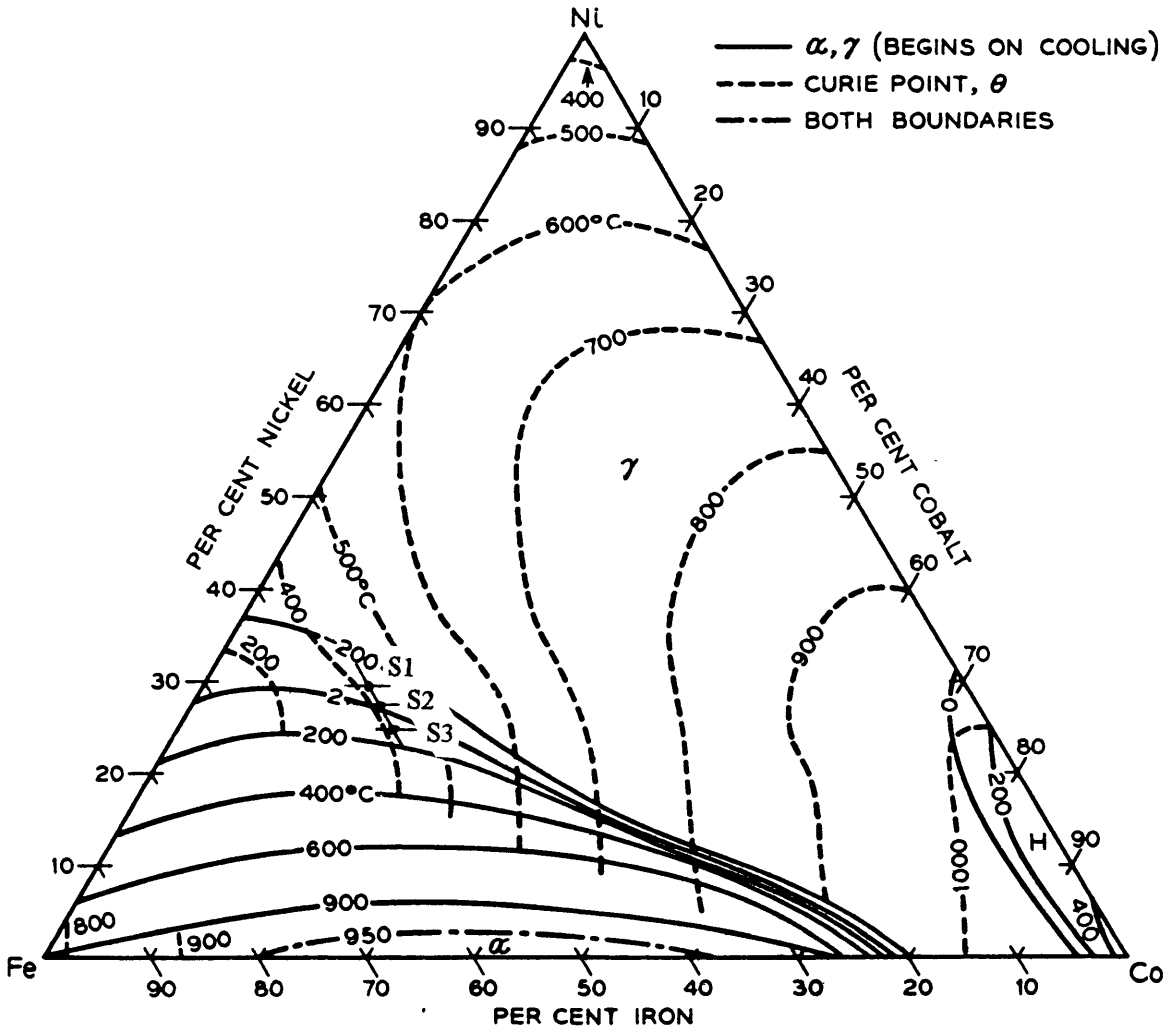


**Figure 1-4 Ternary map of martensite start temperature and Curie temperature (Compositions of three alloys investigated in this research are marked) [17].**

# 2 Experimental Procedures

30 g buttons of the three alloy compositions listed in Table 1-1 were arc-melted under Ar atmosphere. After hot rolling at 1273 K with a reduction of about 60 %, these ingots were homogenized at 1473 K for 24 h in Ar atmosphere and water quenched. Specimens were next ausaged at 873 K or 973 K for 1 h, 3 h, or 10 h, and water quenched. Specimens that showed austenite at room temperature after homogenization or aging were quenched in liquid nitrogen to cause martensitic transformation. As a nomenclature in this thesis, a "homogenized" specimen means as-homogenized but unaged, and an "ausaged" specimen means homogenized and ausaged.

Microstructures were observed in optical microscope and ElectroScan E3 scanning electron microscope (SEM) after being etched with a solution of 75 ml HCl, 75 ml ethanol, 15 g $CuSO_4$, and 15 ml water. Transmission electron microscope (TEM) observation by JEOL 200CX at an acceleration voltage of 200 keV was also carried out to examine martensite substructures and precipitates. TEM specimens were electropolished in a solution of ethanol with 10% $HClO_4$. The chemical composition of precipitates was measured by EDX in a Vacuum Generators HB603 scanning transmission electron microscope (STEM). Compositions reported are the average of values measured in five precipitates located in very thin regions of a TEM specimen. Hardness was measured by a Vickers hardness tester at 4.9 MPa (500 gf) load. Stress-strain curves were measured in compression tests by Instron multi-purpose tester with specimen dimensions of about 8 x 8 x 4 $mm^3$. Saturation magnetization and transformation temperatures were measured by

Digital Measurement Systems 880 vibrating sample magnetometer (VSM). Tetragonality and texture of bulk specimens with a polished surface of about 8 x 8 $mm^2$ were measured by X-ray diffractometry with Cu $K_\alpha$ radiation.

Bend tests of homogenized S1 and S3 were carried out to examine their conventional shape-memory response. Specimens of 33.0 x 2.7 x 0.3 $mm^3$ were cut from bulk samples and were bent by pressing into a V-block in liquid nitrogen. The shape-memory effect was measured by angular recoveries of these specimens after they were heated to room temperature and after further heating to 873 K. Field-induced strain was evaluated with a strain gauge at room temperature, both parallel to and perpendicular to the magnetic field of 6 kOe (Figure 2-1).

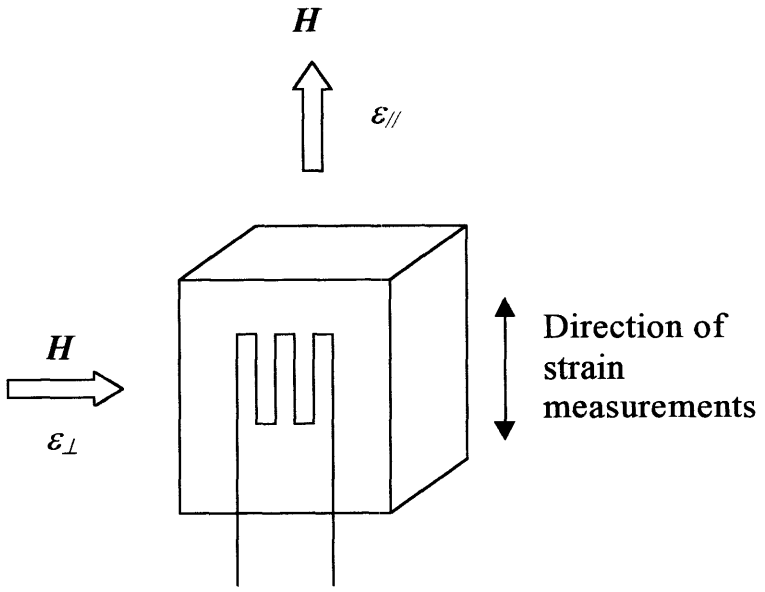


**Figure 2-1 Relative orientations of specimen, strain gauge, and applied magnetic field.**

# 3 Results

## 3.1 Microstructure

After homogenization at 1473 K for 24 h, alloy S1 was austenitic at room temperature and showed austenite twins and grain boundaries (Figure 3-1). S1 aged at 873 K for 1 h still showed austenite at room temperature. However, a specimen aged at 873 K for 3 h (Figure 3-2), as well as other aged specimens (aged at 873 K for 10 h or aged at 973 K) showed lenticular martensite. Therefore, aging alloy S1 effectively increases the martensite start temperature ($T_{Ms}$). Grain size was roughly around 300 μm. Two specimens, one homogenized and one aged at 873 K for 1 h showing austenite at room temperature, were quenched in liquid nitrogen to cause martensitic transformation and then observed at room temperature. The homogenized specimen showed a mixed structure of thin-plate martensite and austenite even at room temperature (Figure 3-3). The aged specimen also showed a fully martensitic structure after quenching in liquid nitrogen (Figure 3-4). However, in this case, the martensite was not typical thin-plate, but seemed to be a mixture of lenticular and thin-plate martensite.

A homogenized specimen of alloy S2 was also austenitic at room temperature. After hardness testing such specimens with a Vickers indenter, stress-induced martensite is visible around the hardness indentations. However, S2 aged at 873 K for 1 h as well as other aged specimens showed lenticular martensite. In the case of alloy S3, not only aged specimens but also a homogenized specimen showed lenticular martensite at room temperature (Figure 3-5).

From these results, both the increase of Co/Ni ratio from S1 to S3 and ausaging promoted the martensitic transformation and increased $T_{Ms}$. SEM observation (Figure 3-6) revealed microstructure of S3 aged at 973 K for 3 h with midrib and 'veins' like precipitates (especially evident in Figure 3-6(b)). Since S3 was already martensitic before ausaging, the second phase (precipitates) seems to nucleate at the defects in martensite substructure, such as twin boundaries or possibly slip bands. Precipitates might be austenite newly formed at the aging stage because the volume fraction of precipitates was too high to be assumed $(Fe,Ni,Co)_3Ti$ precipitates. The Fe-Ni-Co Phase diagram [18] indicates that these alloys probably lie in a two-phase (austenite and ferrite) region at the aging temperature (Figure 3-7) even though the effect of Ti and $(Fe,Ni,Co)_3Ti$ precipitates on the austenite/ferrite equilibrium is unknown.


**Figure 3-1 Optical micrograph of homogenized S1.**

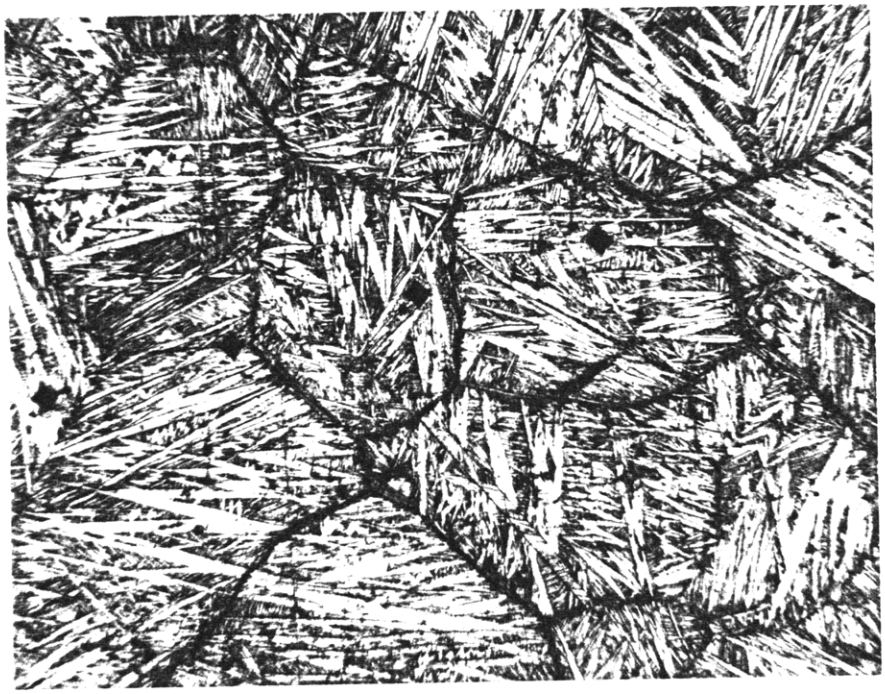


**Figure 3-2 Optical micrograph of S1 aged at 873 K for 3 h.**

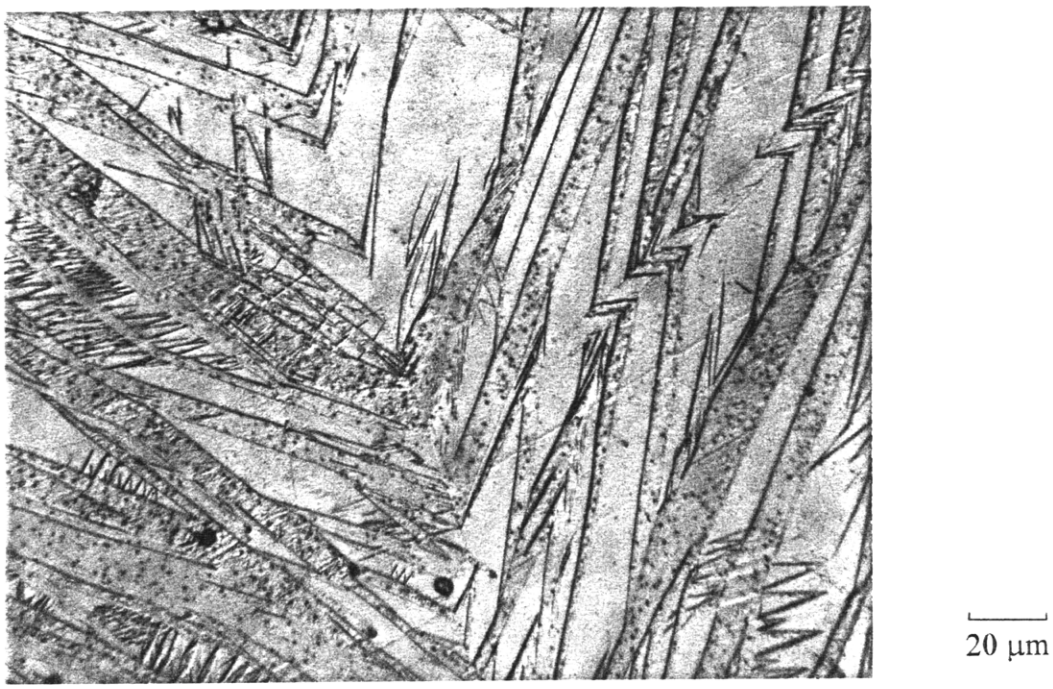


**Figure 3-3 Optical micrograph of homogenized S1 followed by quenching in liquid nitrogen.**

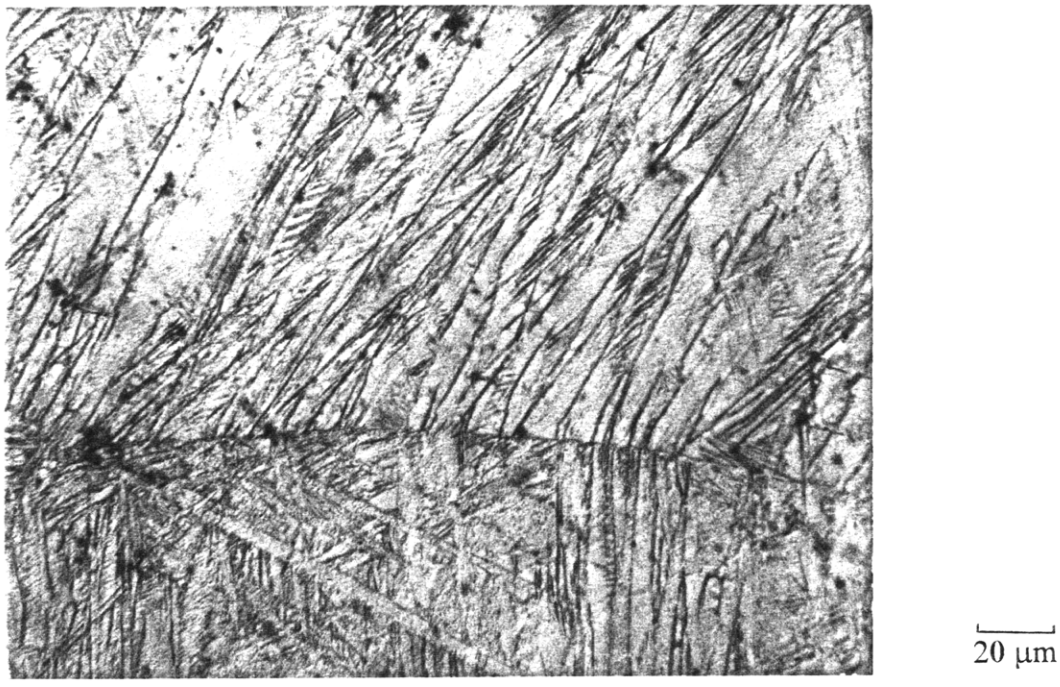


**Figure 3-4 Optical micrograph of S1 aged at 873 K for 1 h followed by quenching in liquid nitrogen.**

(a)

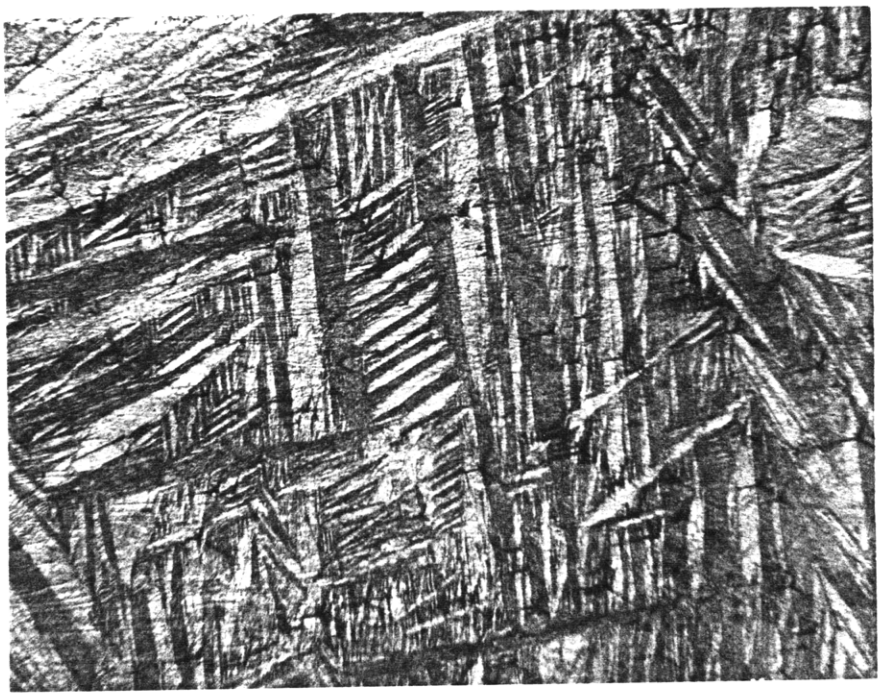

100 μm

(b)

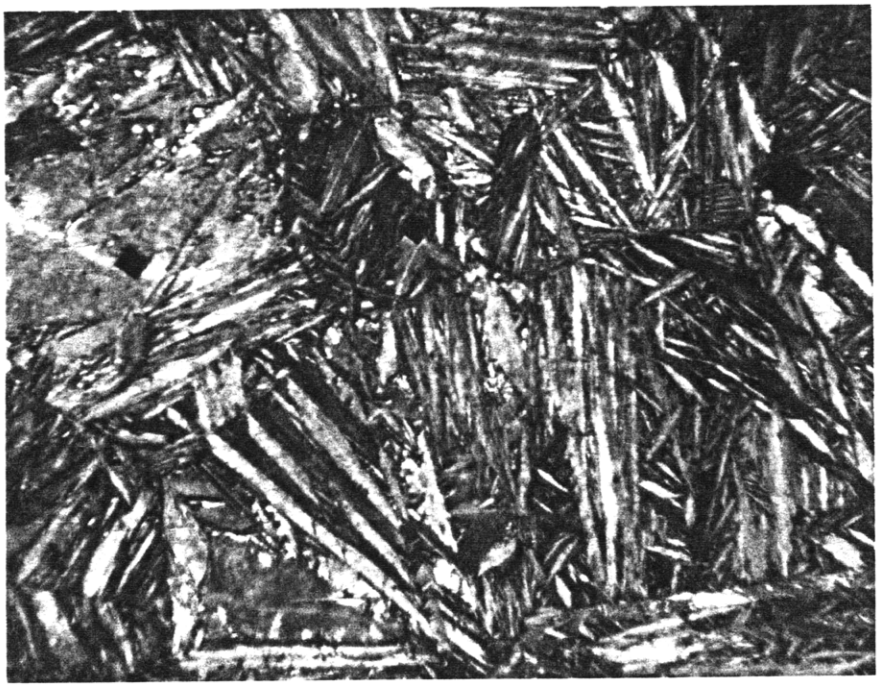

100 μm

**Figure 3-5 Optical micrographs of (a) homogenized S3, (b) S3 aged at 973 K for 3 h.**

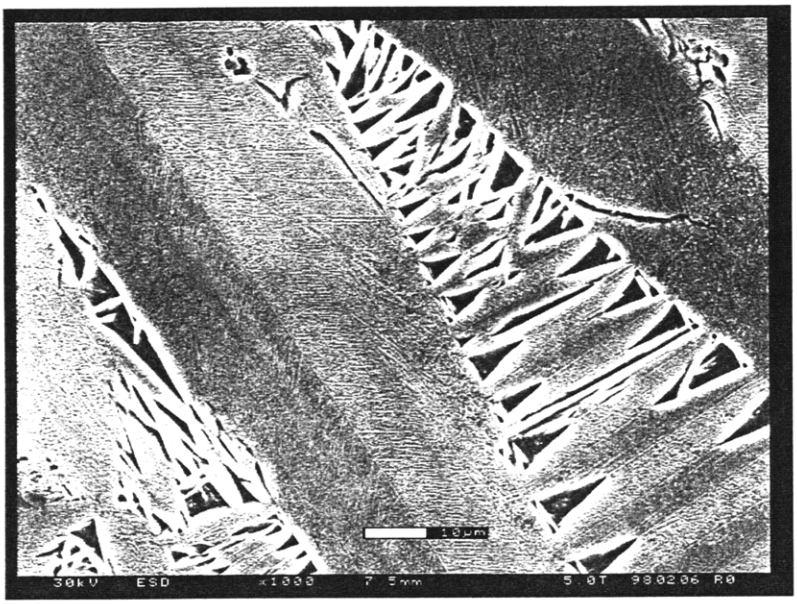


(a)

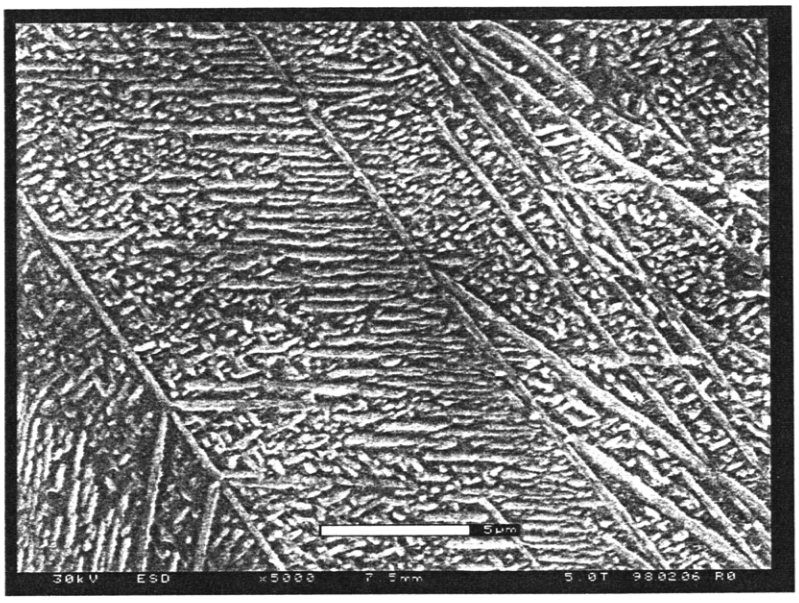


(b)

**Figure 3-6 SEM micrographs of S3 aged at 973 K for 3 h.**

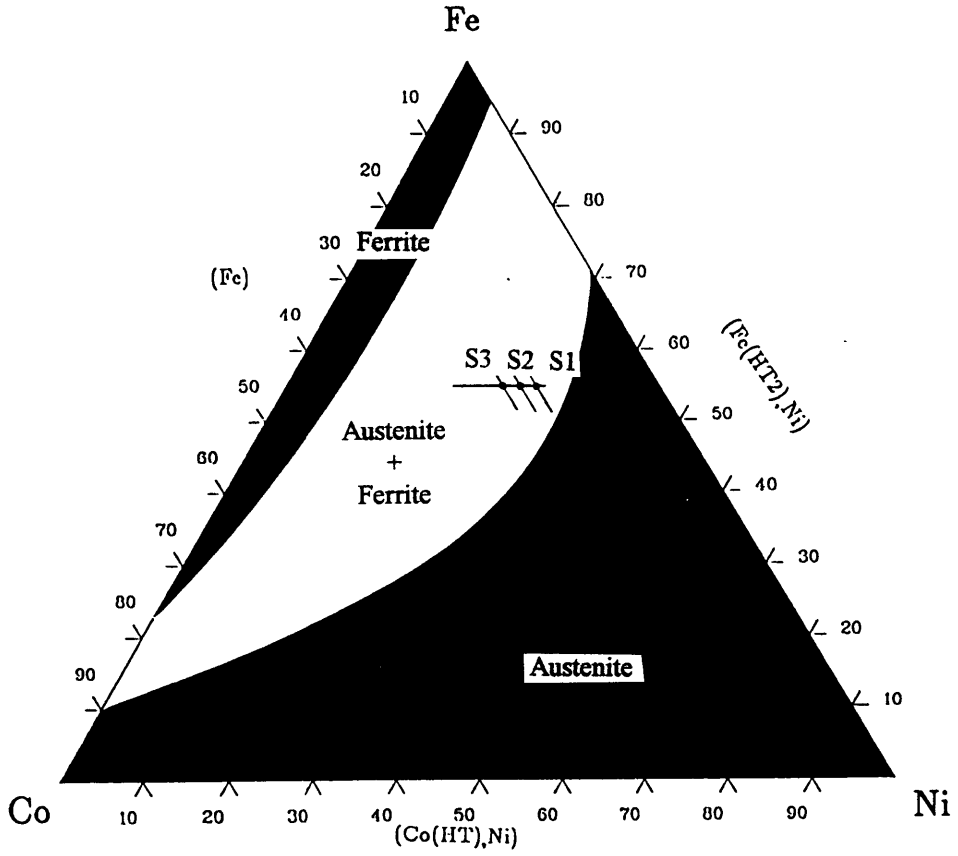


**Figure 3-7 Fe-Ni-Co phase diagram at 973 K (Compositions of three alloys investigated are marked) [18].**

## 3.2 TEM observation

Figure 3-8 is a TEM observation of thin-plate martensite (homogenized S1 after quenching in liquid nitrogen) revealing thin-plate martensite and austenite structure. Transformation twins in the thin-plate martensite extend completely across the thin dimension of a martensite plate and no midrib was observed, as seen in [9]. Such twinned substructure of martensite was not observed in TEM specimens of typical lenticular martensite of S2 aged at 973 K for 10 h.

On the other hand, $(Fe,Ni,Co)_3Ti$ precipitates were observed in S2 aged at 973 K for 10 h (Figure 3-9). These precipitates were evenly distributed and their diameters were in the range of 15-20 nm. EDX measurement in STEM observation of the chemical compositions of these precipitates are given in Table 3-1; this result confirmed that they were likely $(Fe,Ni,Co)_3Ti$-type $\gamma'$ precipitates, based on the content of Ti and the finding that the major element was Ni.

**Table 3-1 Chemical composition of $(Fe,Ni,Co)_3Ti$ precipitates**

**(Average of five precipitates, at%)**

| Fe | Ni | Co | Ti |
|---|---|---|---|
| 7.57 | 57.33 | 10.73 | 24.37 |

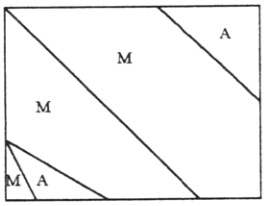


M; Martensite
A; Austenite

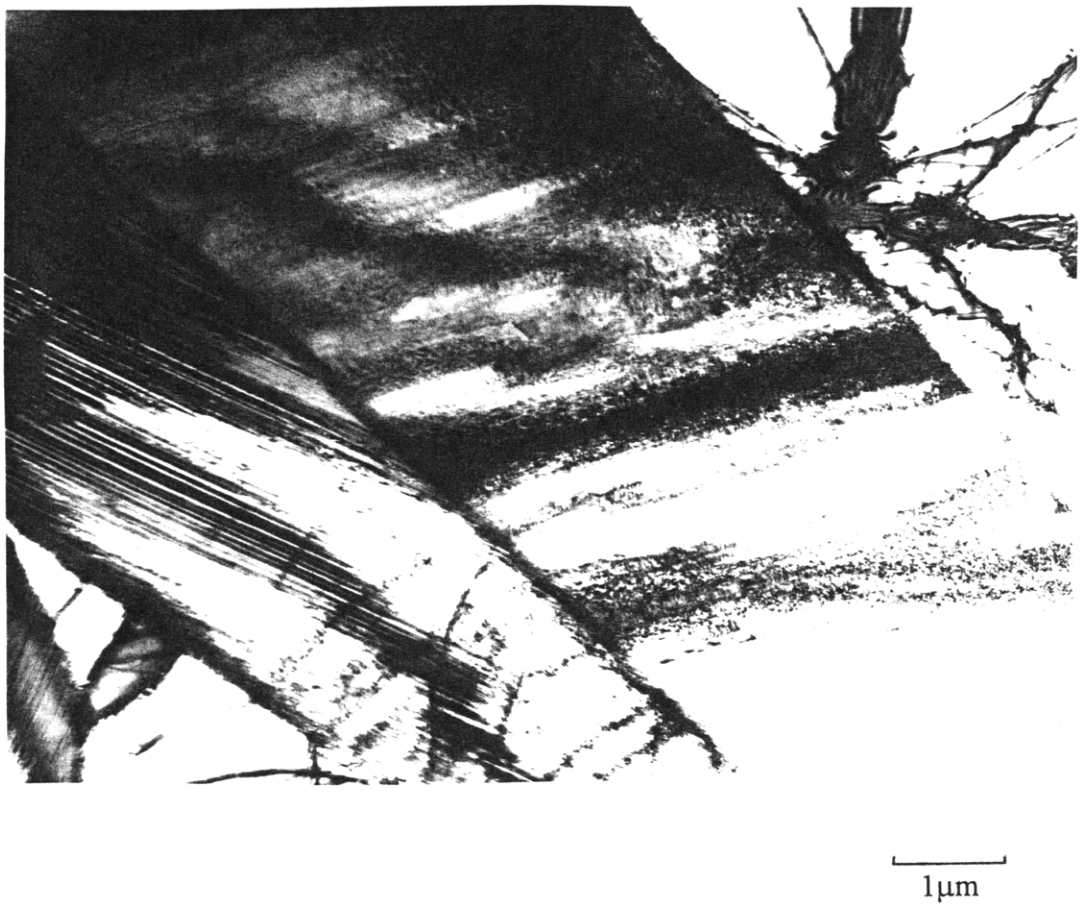


**Figure 3-8 Twinned martensite plates in homogenized S1 after quenching in liquid nitrogen.**

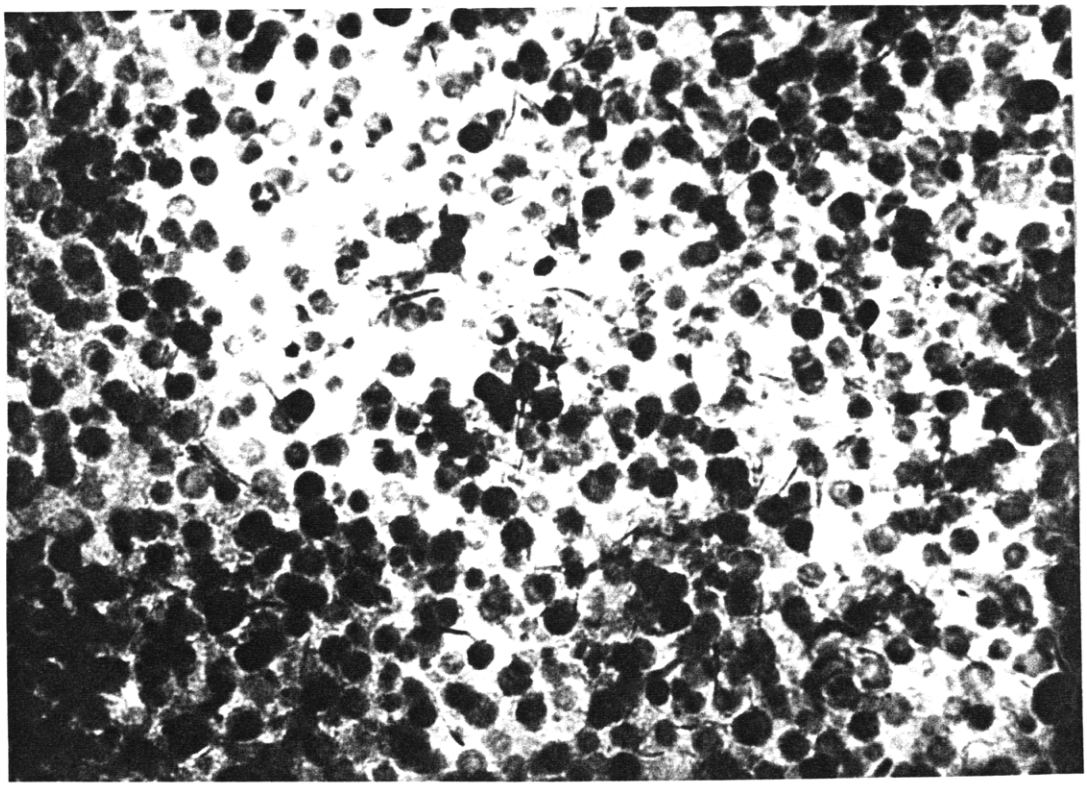


**Figure 3-9 $(Fe,Ni,Co)_3Ti$ precipitates in S2 aged at 973 K for 10 h.**

## 3.3 Hardness

The hardness variation with aging at 873 K or 973 K is shown in Figure 3-10. Ausaging at either temperature effectively increased hardness. While 873 K aging of alloys S1 and S2 showed a continuous increase of hardness with increase in aging time, 873 K aging of alloy S3 showed an aging peak at 1 h or less and a continuous decrease of hardness with further increases in aging time. In the case of 973 K aging, S1 showed an aging peak at 3 h, while S2 and S3 showed aging peaks at 1 h or less and a continuous decrease of hardness with further increase in aging time. These results reveal that increased Co/Ni ratio (S1 to S3) accelerates the aging kinetics. This hardening is thought to be mainly due to the precipitation hardening by $(Fe,Ni,Co)_3Ti$, as shown in TEM observation (Figure 3-9).

Figure 3-11 shows the results of an Instron test on S1 aged 10 h at 973 K. This sample remained stiff up to much higher stresses than polycrystalline $Ni_2MnGa$ samples. This is good for the large actuation force of Fe-Ni-Co-Ti, but also it means that Fe-Ni-Co-Ti alloys will require higher magnetic driving force to move twin boundaries and deform the material.

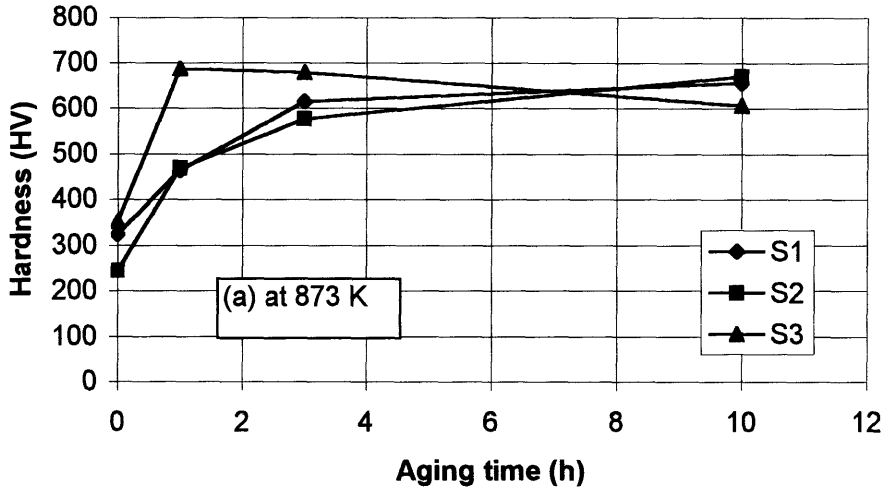


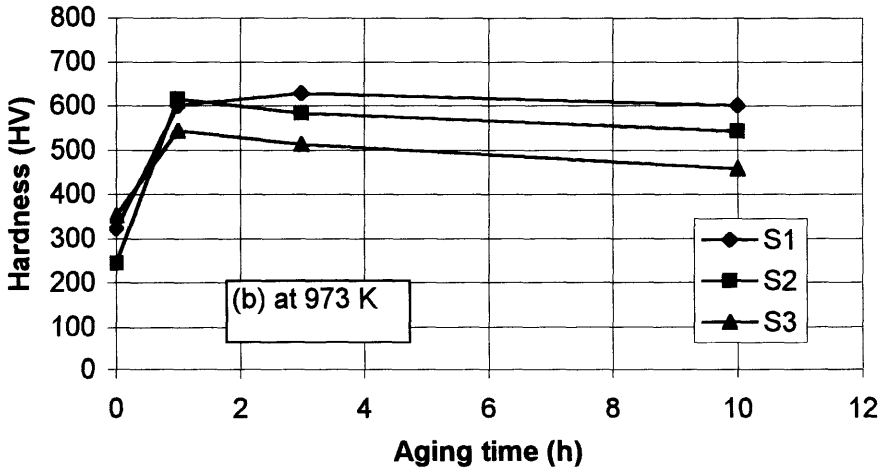


**Figure 3-10 Aging behavior (a) at 873 K and (b) at 973 K.**

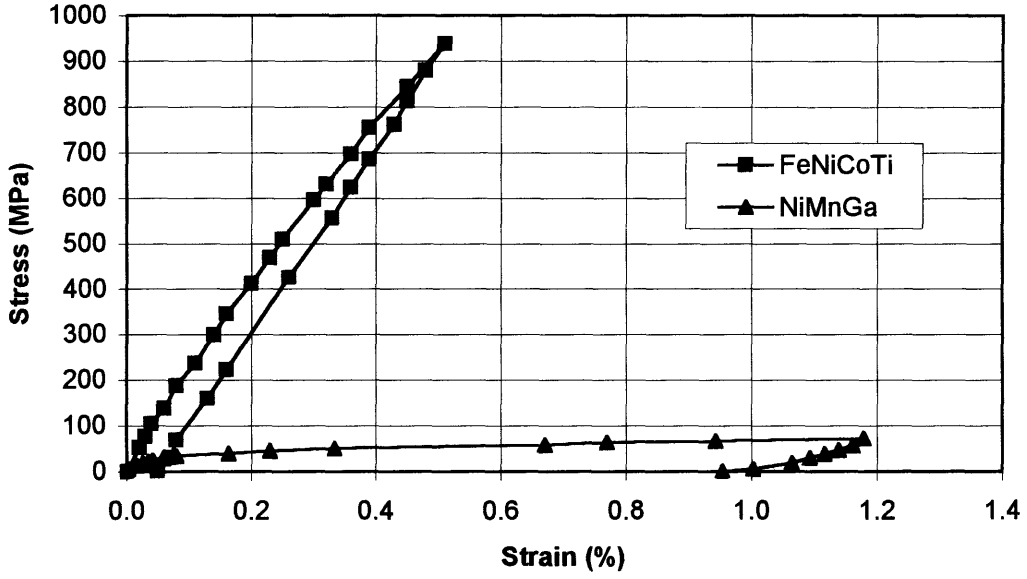


**Figure 3-11 Stress-strain curve of Fe-Ni-Co-Ti (S1 aged at 973 K for 3 h) and $Ni_2MnGa$ (courtesy of S.Murray).**

### 3.4 Transformation temperature

As shown above, martensite start temperatures are sensitive to chemical composition and ausaging treatments. Changes in magnetization with temperature can reveal the martensite-austenite transformation because austenite and martensite exhibit different magnetization behavior. In the case of Fe-Ni-Co-Ti, martensite shows smaller magnetization at a low magnetic field than austenite. Examples of *M-H* loops are shown in Figure 3-12. Figure 3-13 is the magnetization-temperature (*M-T*) curve of homogenized S1, indicating $T_{Ms}$ at 203 K, austenite start temperature ($T_{As}$) at 233 K, and austenite finish temperature ($T_{Af}$) at 348 K. Since $T_{Af}$ is higher than room temperature, homogenized S1 showed martensite even at room temperature after quenching in liquid nitrogen, as seen in Figure 3-3. On the other hand, specimens, which were martensitic at room temperature, maintained *M-H* loops typical for martensite and did not retransform to austenite up to 573 K (Figure 3-14). The transformation temperatures are shown in Table 3-2; thus, both the increase of Co/Ni ratio (from S1 to S3) and ausaging increased transformation temperatures. Although the Fe-Ni-Co phase diagram illustrates that an increase of Co/Ni ratio leads to an increase of $T_{Ms}$, the current result shows the same trend even with Ti and $(Ni, Co, Fe)_3Ti$ precipitates (Figure 1-4). Moreover, this result indicates that it is possible to obtain martensite at or above room temperature with proper choice of chemical composition and ausaging.

The results of *M-T* loops (Figures 3-13 and 3-14) also showed that the Curie temperatures of all of these alloys were higher than 473 K, regardless of ausaging. Therefore, these alloys have sufficiently high Curie temperatures for practical applications.

**Table 3-2 Transformation temperatures (K)**

| Alloy | Heat treatment | $T_{Ms}$ | $T_{Mf}$ | $T_{As}$ | $T_{Af}$ |
|---|---|---|---|---|---|
| S1 | Homogenized | 203 | <123 | 233 | 348 |
| S1 | Ausaged at 873 K for 1 h | 243 | 173 | 333 | Not detected |
| S1 | Ausaged at 873 K for 10 h | >573 | Not detected | >573 | Not detected |
| S3 | Homogenized | >573 | Not detected | >573 | Not detected |

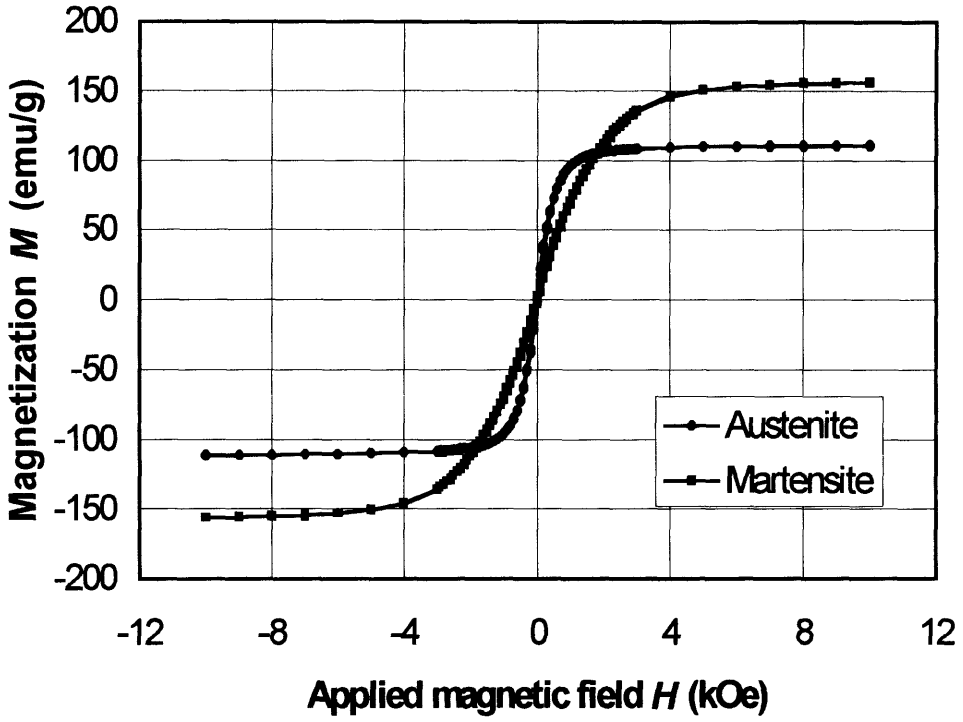


**Figure 3-12** ***M-H*** **loops of austenite (homogenized S1) and martensite (S1 aged at 873 K for 10 h).**

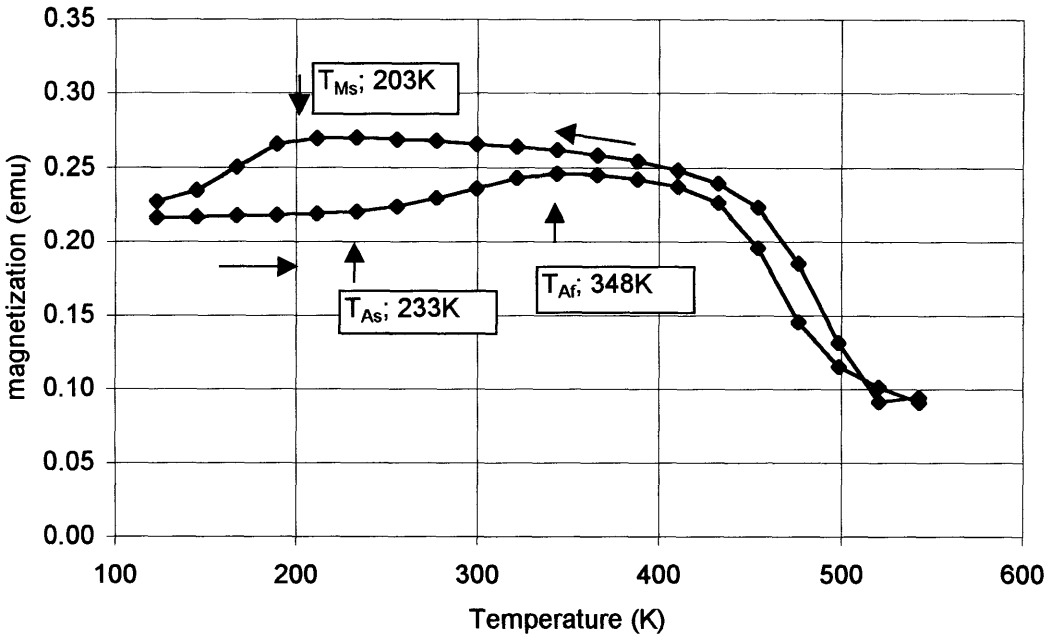


**Figure 3-13** ***M-T*** **loop of homogenized S1.**

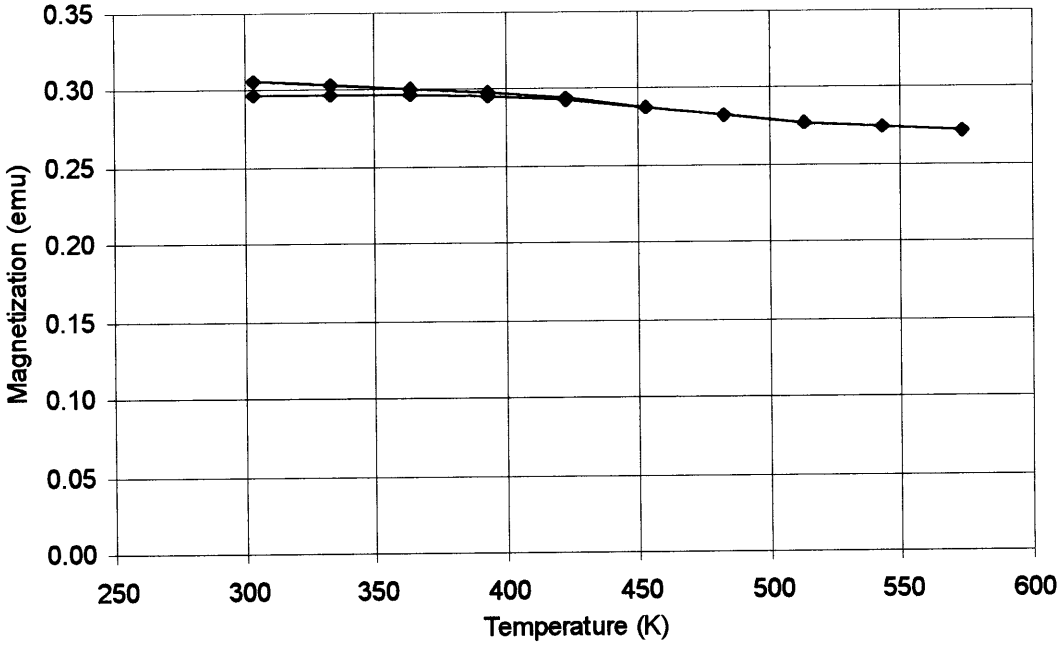


**Figure 3-14 *M-T* loop of S1 aged at 873 K for 10 h.**

### 3.5 Saturation magnetization

Figure 3-12 showed that martensite exhibited higher saturation magnetization ($M_s$) and magnetocrystalline anisotropy energy than austenite. Figure 3-15 shows the variation of $M_s$ with various aging conditions and that the aging of S1 and S2 increased $M_s$ dramatically. Specimens composed of martensite showed a saturation magnetization of more than 140 emu/g, while those mainly composed of austenite showed less than 130 emu/g. On the other hand, $M_s$ of martensite was almost constant with aging time; longer time aging and aging of martensite (in the case of S3) were not effective to increase $M_s$. As a result, $M_s$ can be increased through martensitic transformation, but once martensite is obtained, $M_s$ does not increase further.

The effect of chemical composition is also seen in Figure 3-15; S1 showed slightly smaller $M_s$ compared to S2 and S3 regardless of aging conditions. The current results on Fe-Ni-Co-Ti show the same trend in magnetization as indicated in the Fe-Ni-Co phase diagram, that is, $M_s$ increases with increasing Co/Ni ratio (Figure 3-16) [17].

Values of $M_s$ of S3 around 160 emu/g are three times larger than that of $Ni_2MnGa$ (58 emu/g [5]) and thus will produce three times the magnetic pressure on the twin boundaries for a given field [19].

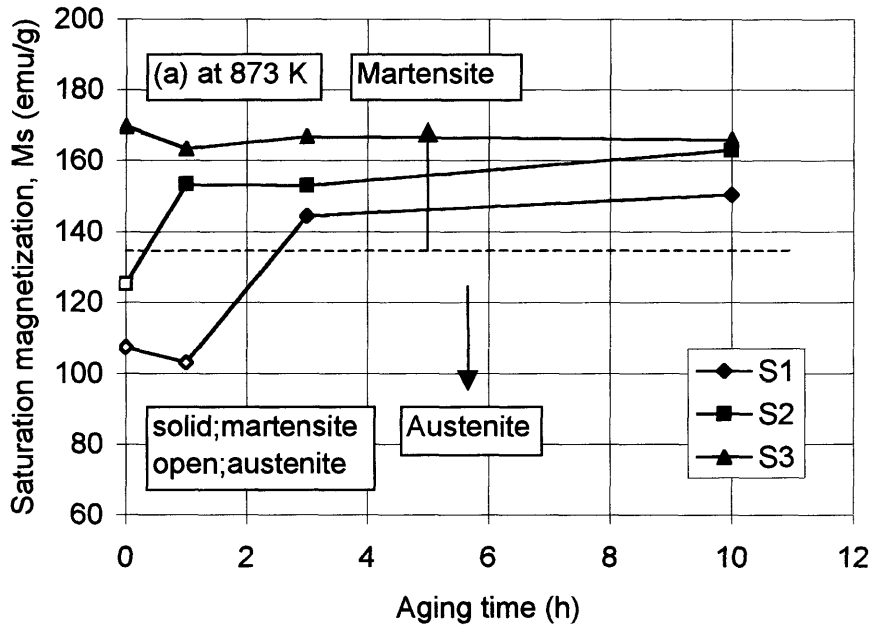


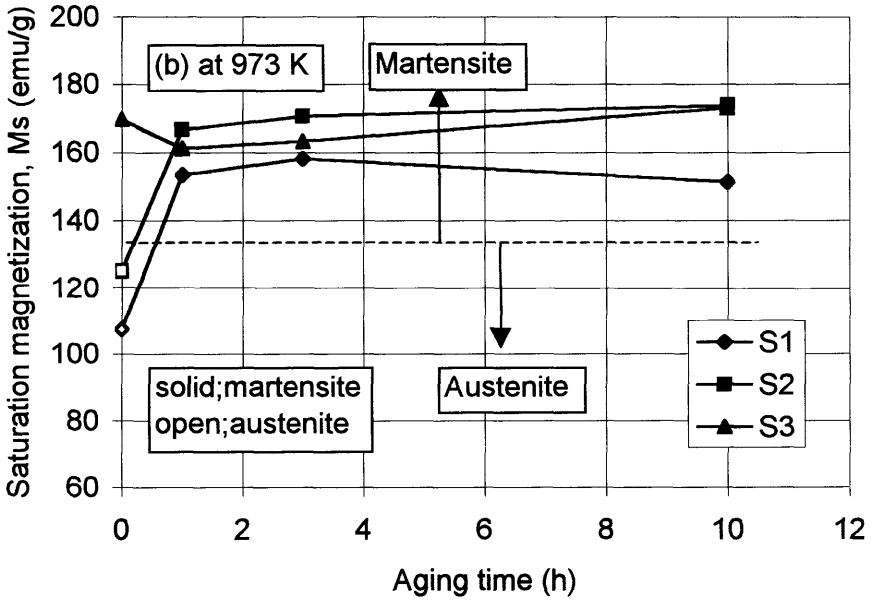


**Figure 3-15 Aging behavior on saturation magnetization.**

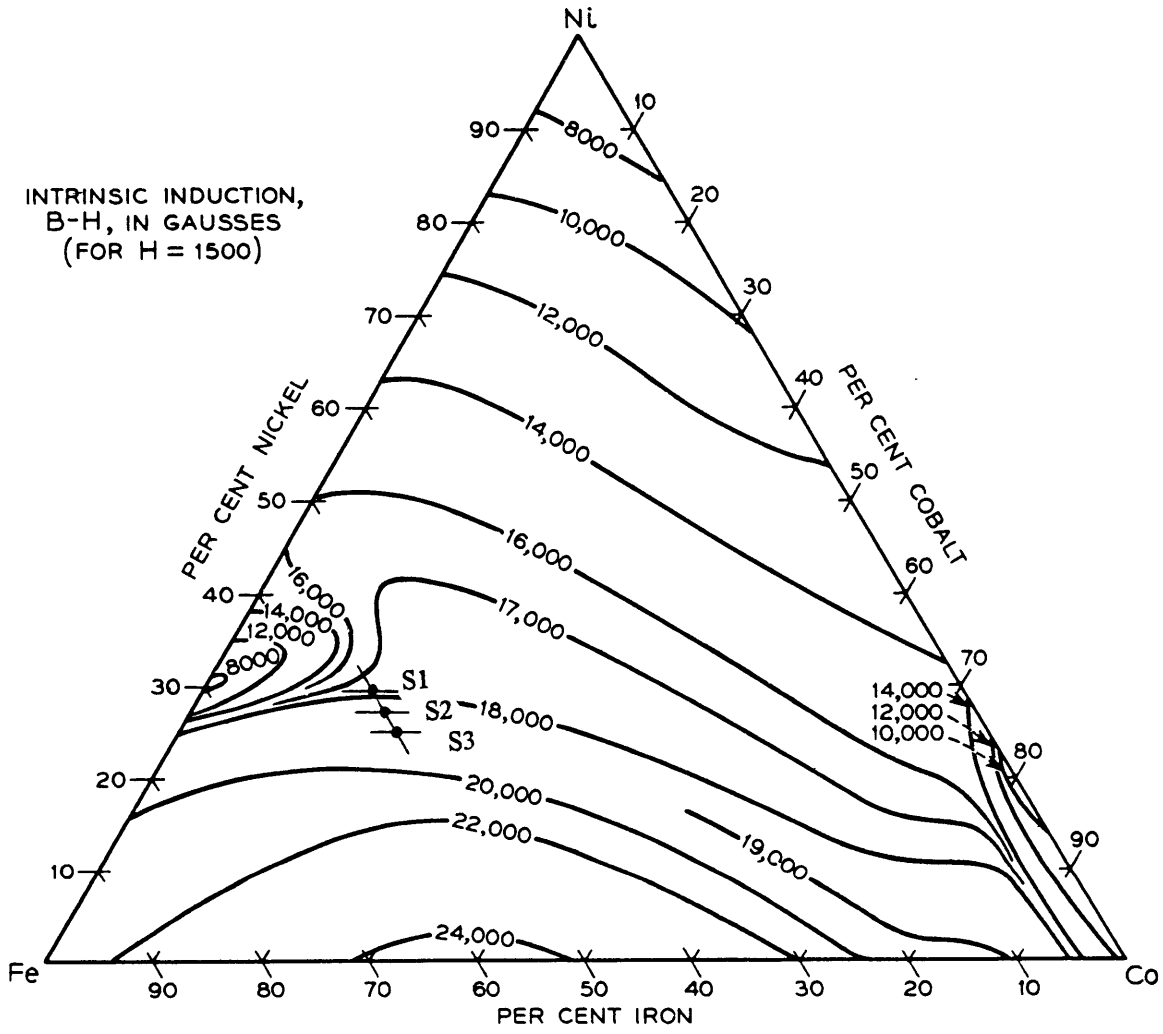


**Figure 3-16 Saturation magnetization of annealed Fe-Ni-Co alloys [17].**

### 3.6 X-ray measurement

X-ray diffractometer scans of selected specimens (grain size was around 300 μm, see Figure 3-2) did not show measurable tetragonality (Figure 3-17). Also, significant texture due to hot rolling was not detected in these specimens since the relative peak intensities did not deviate significantly from those expected from powder standard samples.

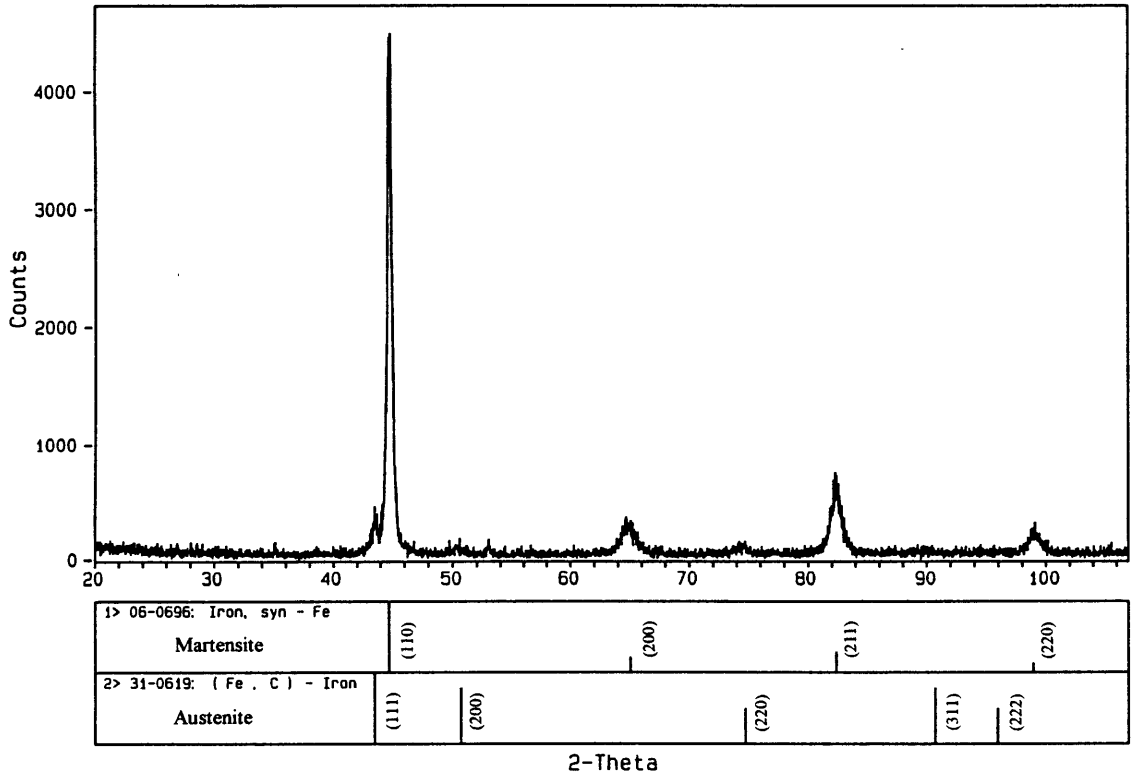


**Figure 3-17 X-ray diffraction of S2 aged at 973 K for 10 h.**

## 3.7 Shape-memory effect

Conventional shape-memory response was examined with specimens of homogenized S1 and S3 to compare the effect of martensite morphology. Figure 3-18 presented the angular recoveries at each temperature. Thin-plate martensite of homogenized S1 showed a significant shape-memory response; on the other hand, lenticular martensite in homogenized S3 showed very little shape recovery. Thus, it is confirmed that thin-plate morphology is required for conventional shape-memory effect and that the twinned structure of thin-plate martensite works to show shape-memory effect. Therefore, it can be concluded that the twinned structure of homogenized S1 has the potential to show MSM effect based on its mechanism.

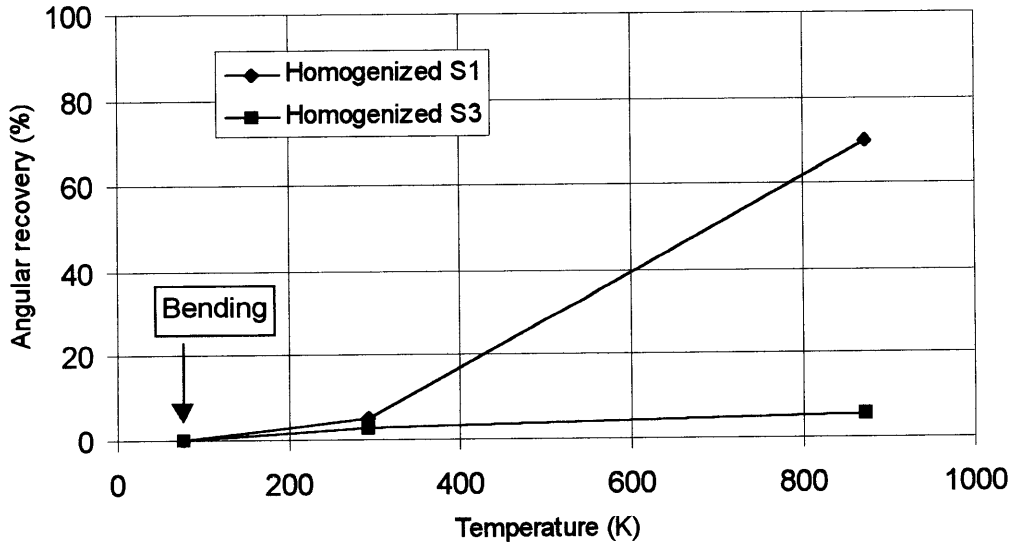


**Figure 3-18 Shape memory effect.**

### 3.8 Field-induced strain

Austenitic specimens, such as homogenized S1, S1 aged at 873 K for 1 h, and homogenized S2, showed identical strain-field ($\varepsilon$-$H$) loops, all having inflection points (Figure 3-19). Strains parallel to the magnetic field started to increase at around 1 kOe, and kept increasing up to 6 kOe. Strains perpendicular to the magnetic field started to increase at around 2 kOe. At maximum magnetic field of 6 kOe, strains in both directions did not show saturation. The field-induced strains, which are identified as the differences of strains parallel to and perpendicular to the magnetic fields at 6 kOe ($\varepsilon_{//}$-$\varepsilon_{\perp}$), were around 10 ppm. Since these materials were austenitic at room temperature, the measured strains are thought to arise from the magnetostriction of the austenitic phase instead of the MSM effect in the martensitic phase.

The results of field-induced strain measurements in martensitic specimens are divided to two groups depending on their heat treatments. Overaged specimens (aged beyond the peak at each temperature, such as S2 aged at 973 K and all aged S3) showed $\varepsilon$-$H$ loops as seen in Figure 3-20. These loops are characterized by early saturation at around 3 or 4 kOe, positive strain measured parallel to the magnetic field, and negative strain measured perpendicular to the magnetic field. The field-induced strains were found to be around 40 ppm.

Underaged specimens (such as S1 and S2 aged at 873 K) showed $\varepsilon$-$H$ loops similar to those of the overaged specimens (Figure 3-21). However, these underaged loops were characterized by late saturation; these specimens did not show strain saturation even at maximum field. The amounts of strains were around 30 ppm and were smaller than those of overaged specimens. Late saturation may account for the smaller level of

strains. The directions of the strains relative to the directions of magnetic field were the same as those seen in the overaged specimens.

The results of homogenized martensitic specimens were not identical; S1 quenched in liquid nitrogen, which showed thin-plate martensite, exhibited an $\varepsilon$-$H$ loop (Figure 3-22) similar to those of the underaged specimens, while S2 quenched in liquid nitrogen and S3 showed $\varepsilon$-$H$ loops similar to those of the overaged specimens.

Regardless of morphology of martensite, the magnitudes of field-induced strains observed in all Fe-Ni-Co-Ti specimens were very small compared to current actuator materials.

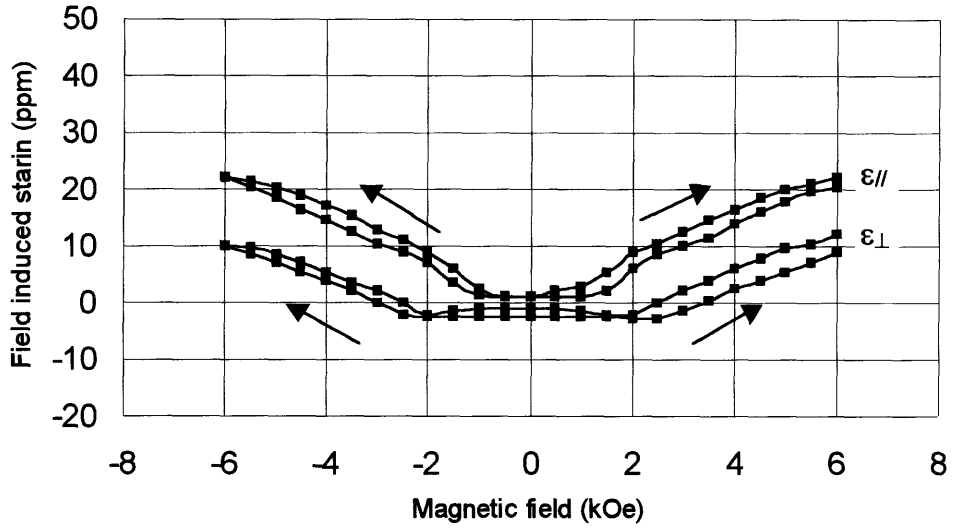


**Figure 3-19 Field-induced strain in homogenized S1.**

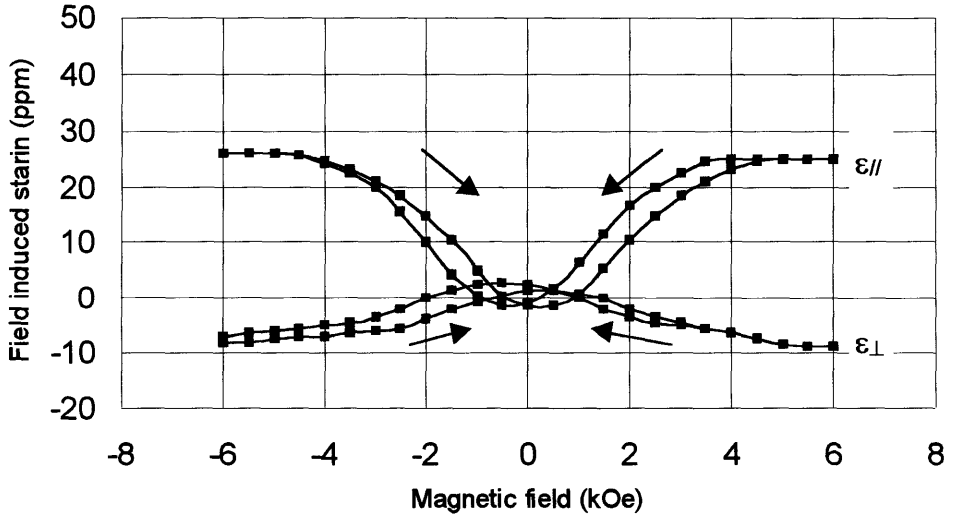


**Figure 3-20 Field-induced strain in S3 aged at 973 K for 1 h.**

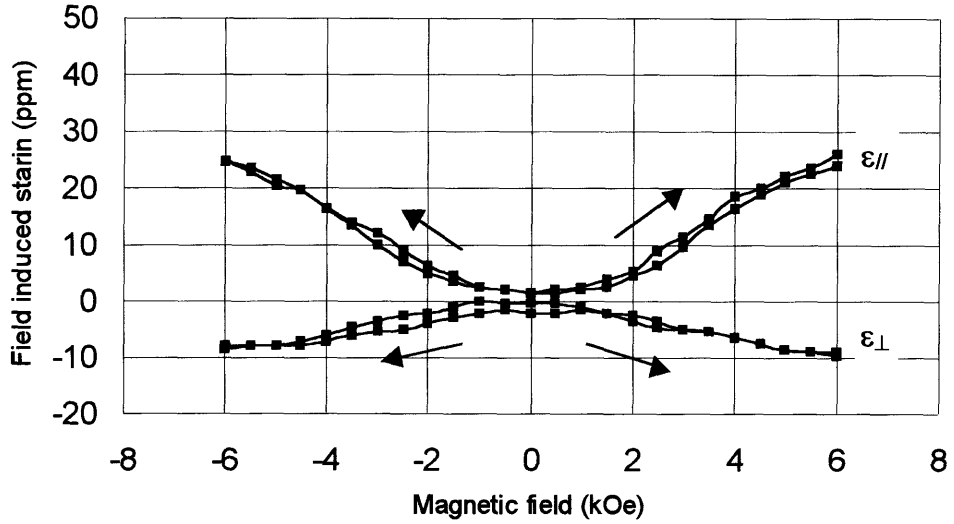


**Figure 3-21 Field-induced strain in S1 aged at 873 K for 10 h.**

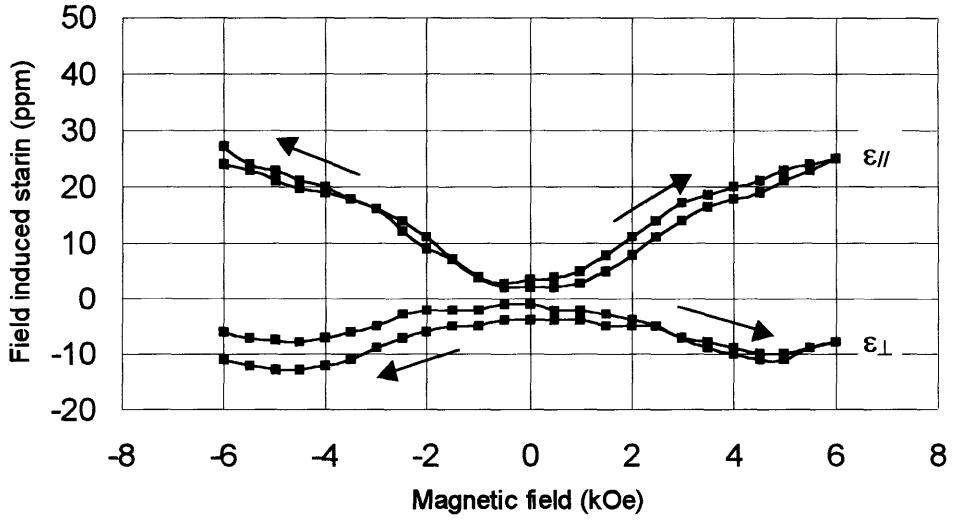


**Figure 3-22 Field-induced strain in homogenized S1 followed by quenching in liquid nitrogen.**

# 4 Discussion

## 4.1 Martensite morphology

As shown in Figures 3-2 to 3-5, two types of martensite morphology, thin plate and lenticular, were observed in this research. Thin-plate martensite was obtained only in a homogenized S1 specimen followed by quenching in liquid nitrogen. The characteristics of these two types of martensite are summarized in Table 4-1 [9].

**Table 4-1 Characteristics of thin-plate and lenticular martensite [9]**

| Thin-plate martensite | Lenticular martensite |
|---|---|
| Absence of midrib. | With midrib. |
| Transformation twins completely extend from one end to the other. | Transformation twins locally exist in the vicinity of midrib. |
| No apparent accommodation slip in surrounding austenite; austenite elastically accommodates the shear and volume strain. | Surrounding austenite is deformed. |
| Necessary for thermoelastic transformation. | |
| Martensite interface is glissile. | |
| Highly smooth and planar interfaces. | |

According to phenomenological crystallographic theory (Wechsler, Lieberman, and Read [4]), martensitic transformation is composed of three basic deformations: (1) a Bain distortion for the necessary lattice change, (2) a shear deformation (lattice-invariant shear), which produces undistorted habit plane, and (3) a rotation of the transformed

lattice, so that the undistorted habit plane has the same orientation in both the parent and product crystals. The second step, lattice-invariant shear, can occur in either slip or twinning. Though slip is not reversible since atoms near dislocations lose their positional relation with neighboring atoms, twinning can be reversible because atoms in twinning deformation do not lose their relative position with neighboring atoms. Consequently, twinned martensite can show shape reversibility.

My results and those of Maki [9] showed that thin-plate martensite is completely twinned and lenticular martensite has little or a small amount of twinning. Thus, thin-plate martensite can be assumed twinned martensite. As explained in the introduction, MSM materials require twinned martensite since the reorientation of twin variants is thought to be the mechanism of MSM effect. Therefore, thin-plate martensite is required for MSM materials. Thus, thin-plate martensite can theoretically show shape reversibility, and our observations of conventional shape memory behavior in Fe-Ni-Co-Ti alloys correlates with the thin-plate martensitic morphology.

## 4.2 Promotion of twinned (thin-plate) martensite at or above room temperature

As explained above, twinned martensite substructure is required for MSM materials. There are several ways to obtain twinned (thin-plate) martensite:

A. Decrease martensite start temperature ($T_{Ms}$) [20, 21]. This can be achieved by means of a suitable combination of Fe, Ni, and Co.

B. Decrease stacking fault energy [22].

C. Decrease the critical resolved shear stress required for twinning [23].

D. Increase tetragonality of martensitic phase. This is because high tetragonality makes

the formation of twinning easy upon martensitic transformation. Tetragonality can be increased by (1) increasing Ti [24], (2) alloying a suitable combination of Fe, Ni, and Co [9, 25], (3) ausaging appropriately [9, 12], and (4) applying cold working [12].

E. Decrease transformation volume change, thus reducing strain at the martensite-austenite interfaces, which otherwise would need to be accommodated in surrounding austenite [9].

F. Increase the strength of austenite. High hardness inhibits slip in austenite at martensite-austenite interfaces [9]. Ausaging increases hardness and the addition of precipitate-forming elements, such as Ti and Al, accelerates the aging effects.

Since thin-plate martensite has already been observed in my experiments, the next step is to obtain a large amount of twinned martensite at room temperature. This can be achieved by (1) higher $T_{Ms}$ and (2) increased thermal hysteresis. As seen in Section 3.1, the increase of $T_{Ms}$ by the combination of chemical composition (the increase of Co/Ni ratio) and ausaging was not successful due to the appearance of lenticular martensite. However, based on the previous discussion, increased tetragonality, increased strength of austenite, and the addition of carbon (the effect of carbon is seen in Figure 4-1) [21, 26] can be helpful to obtain twinned martensite with higher $T_{Ms}$.

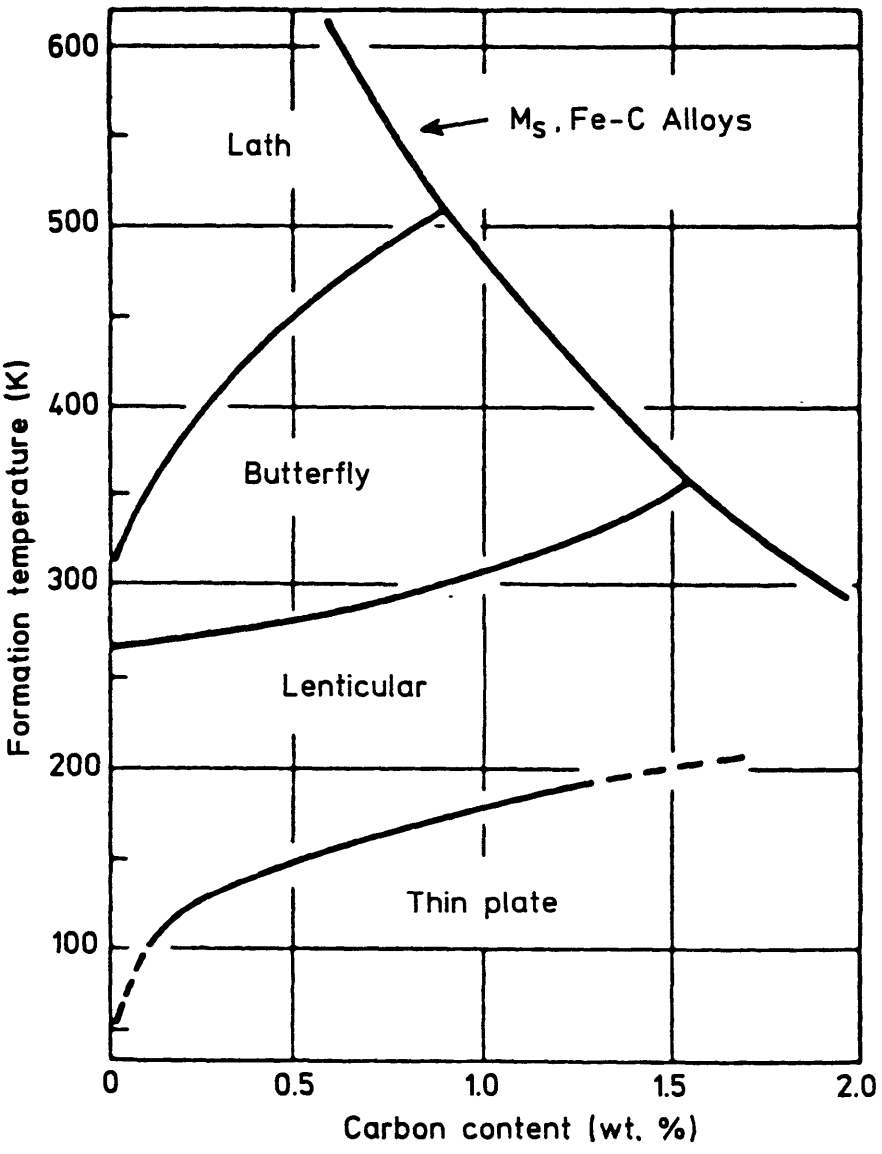


**Figure 4-1 Diagram of martensite morphology and martensite formation temperature in Fe-Ni-C alloys [21, 26].**

## 4.3 Thermal hysteresis

Thermoelastic martensite is characterized by small thermal hysteresis and mobile martensite-austenite interfaces [11]. As seen in Figure 4-2, thermal hysteresis is widely different between thermoelastic (Au-Cd) and non-thermoelastic (Fe-Ni) martensite, and this comes from their magnitudes of shear strain component on martensitic transformation [27]. In the case of non-thermoelastic martensite with a large shear strain component (0.20 in Fe-30Ni), a large free energy is required to start martensitic transformation because a large shear is required to form the martensite. Therefore, a high degree of supercooling is required to produce large free energy; then the thermal hysteresis becomes wide. Since thermoelastic martensite is associated with small shear strain component (0.05 in Au-Cd), required free energy is small; then thermal hysteresis becomes narrow.

Most ferrous alloys show large thermal hysteresis [26], since they are non-thermoelastic martensite with a large transformation strain. However, small hysteresis with almost complete conventional shape memory effect was observed in Fe-Ni-Co-Ti [11, 13, 15], though almost complete shape recoveries with large hysteresis were also reported [10, 14, 15]. At present, the mechanism of the large thermal hysteresis with mobile martensite-austenite interfaces is not clear because large strain induces slip deformation in surrounding austenite at martensite-austenite interfaces.

In current research, homogenized S1, as well as S1 aged at 873 K for 1 h, exhibited large thermal hysteresis as shown in Figure 3-13. Thus, thin-plate martensite of homogenized S1 is categorized in the latter group (shape recovery with large hysteresis) and is not a typical thermoelastic martensite as in the case of [9]. Large thermal hysteresis can be useful to extend the operating temperature of MSM materials because once

transformed to martensite, martensitic phase can remain even at a high temperature with increased thermal hysteresis, although the martensite start temperature is low (Fe-Ni in Figure 4-2). In fact, it is not clear whether MSM materials require mobile martensite-austenite interfaces of thermoelastic martensite, as do shape-memory materials. Based on the mechanism of MSM effect mentioned in the introduction, mobile interfaces may not be required; only twinned substructure is required. Therefore, it can be concluded that large thermal hysteresis may increase the operating temperature of MSM materials as long as twinned structure is maintained. The width of thermal histeresis can be changed by the combination of alloying elements [13, 25]

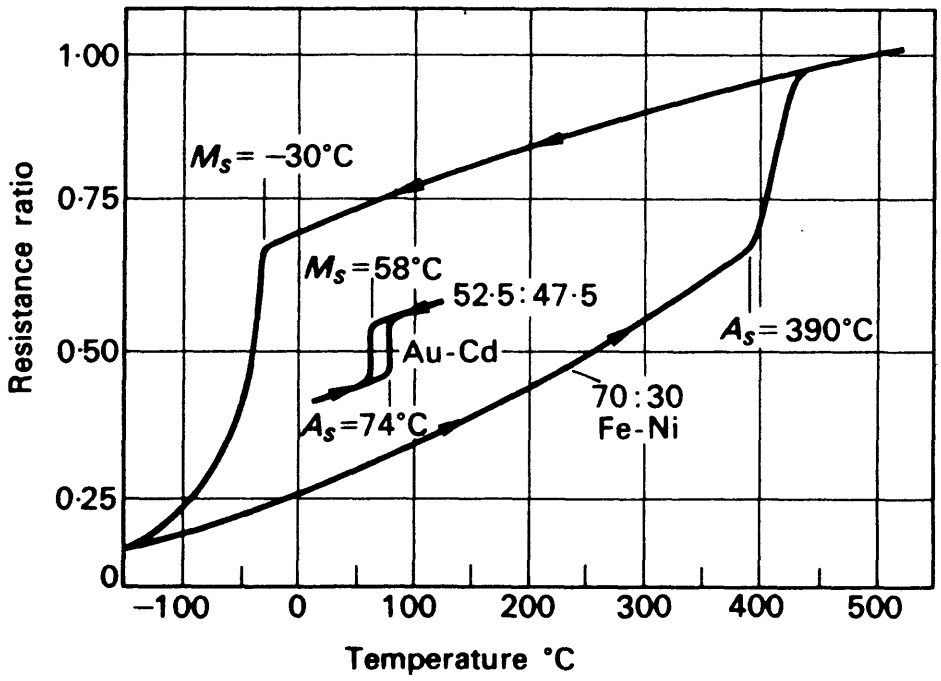


**Figure 4-2 Resistivity changes with temperature in Fe-Ni (non-thermoelastic) and Au-Cd (thermoelastic) alloys [27].**

## 4.4 Increase of $M_s$ from austenite to martensite

As shown in Figure 3-15, the martensitic phase presented higher saturation magnetization ($M_s$). Three factors account for this phenomenon: matrix composition, Curie temperature, and density.

Because of $(Fe,Ni,Co)_3Ti$ precipitates, the matrix of aged specimens may have a lower content of Ti and Ni and a higher content of Fe and Co than that before ausaging. This can result in higher saturation magnetization after ausaging since Fe and Co has higher magnetization. However, this idea would be discarded because homogenized S3 exhibited high $M_s$ without aging (supposedly with no precipitates).

The difference of Curie temperatures can lead to the observed difference in $M_s$ at room temperature. Since $M_s$ starts to decrease when approaching Curie temperature, a material with a higher Curie temperature may show higher $M_s$ than one with a lower Curie temperature at a certain temperature even though both have the same $M_s$ at 0 K. Unfortunately, the Curie temperature of austenite is not detected in this research due to transformation from austenite to martensite on heating.

Another possibility is the density of materials; since higher density generally leads to lower $M_s$, it is reasonable that the austenitic phase with a higher density exhibited lower $M_s$ than a martensitic phase with a lower density.

## 4.5 Balance of stiffness and magnetic energy

MSM behavior strongly depends on the balance of stiffness and magnetic energy of the material, because the reorientation of a unit cell (twin boundary motion) is constrained by the surrounding grains. Recently, O'Handley treated this problem [19] and based on his model, the balance of stiffness and magnetic energy of Fe-Ni-Co-Ti is discussed as follows compared with $Ni_2MnGa$ [5].

Figure 4-3 depicts three representative geometries for two twin variants and an applied magnetic field (above) and the field dependence of magnetization and strain (below), where $M_s$ is the saturation magnetization of each variant; $H$ is the applied magnetic field; $m$ is the magnetization projection along the applied field direction ($m = M/M_s$); $\varepsilon_x$ ($\varepsilon_x = e_x/e_0$) and $\varepsilon_y$ ($\varepsilon_y = e_y/e_0$) are the diagonal components of the strain tensor; $e_0$ is the transformation strain, and $C$ is the effective stiffness. This model assumes that the magnetic anisotropy is much stronger than the Zeeman energy $M_sH$, where large field-induced strain by the MSM effect is expected. See the line of $\varepsilon_y$; the greater $h_e$, the larger strain at any conditions. Therefore, large $M_s$ and small $C$ and $e_0$ are favorable for large field-induced strain at a given magnetic field.

In the current research, Fe-Ni-Co-Ti martensite showed three times as large $M_s$ (Section 3.5) and stiffness (Section 3.3) as that of $Ni_2MnGa$, assuming that the effective stiffness is represented by elastic modulus and that elastic moduli of Fe-Ni-Co-Ti and $Ni_2MnGa$ are about 210 GPa and 60 GPa, respectively. Since the $M_s/C$ ratio becomes the same in both alloys, $h_e$ depends on $e_0$. In fact, $e_0$ affects $\varepsilon_y$ significantly since $h_e \propto e_0^{-2}$. If $e_0$ of Fe-Ni-Co-Ti is assumed to be the same to that of $Ni_2MnGa$, $h_e$ of both alloys becomes almost the same. This implies that Fe-Ni-Co-Ti possesses the potential to

generate the same amount of field-induced strain and stronger force due to its high hardness compared to $Ni_2MnGa$. However, since Fe-Ni-Co-Ti exhibited fairly large thermal hysteresis (Figure 3-13), it may possess large transformation strain [26, 28]. Based on this analysis, alloys in this system with small transformation strain should be explored in future work.

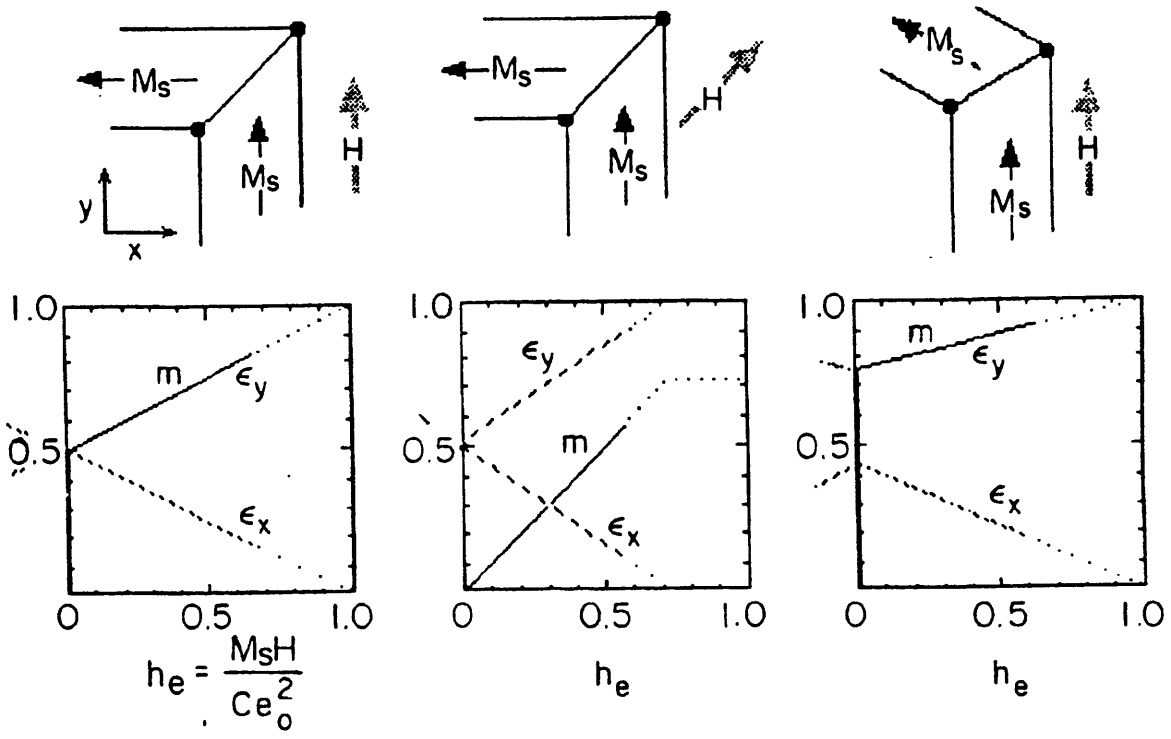


**Figure 4-3 Above, three representative geometries for two twin variants and an applied field. Below, each is displayed the field dependence of magnetization and strain [19].**

## 4.6 Field-induced strain in polycrystalline materials

Recently, one of my colleagues, M. Marioni, made a calculation about the field-induced strains in a single crystal and a polycrystalline material [29]. His calculation was based on O'Handley's model of the MSM effect in a single crystal comprised of only two twin variants [19], but extended the analysis to a polycrystal. His result showed that a polycrystalline material exhibited almost no strain, even though a single crystal of the same material showed some amount of field-induced strain. This is thought to be due to the interference and cancellation of the strains of the differently oriented grains.

## 4.7 Performance of thin-plate martensite

As discussed above, thin-plate martensite has the potential to exhibit the MSM effect; therefore, the MSM performance of thin-plate martensite in Fe-Ni-Co-Ti alloys (homogenized S1 followed by quenching in liquid nitrogen) is of interest. The mechanical and magnetic properties were measured and are summarized in Table 4-2. Unfortunately, even this thin-plate martensite did not show any significant field-induced strain (Figure 3-22). As discussed above, this may be due to the polycrystalline microstructure of the specimen.

**Table 4-2 Mechanical and magnetic properties of thin-plate martensite (homogenized S1 followed by quenching in liquid nitrogen).**

| | |
|---|---|
| Microstructure | A mixture of thin-plate martensite and retained austenite<br>Figure 3-3 (optical microscope observation)<br>Figure 3-8 (TEM observation) |
| Hardness | 450.5 HV |
| Saturation Magnetization ($M_s$) | 121.45 emu/g |
| X-ray diffraction | Figure 4-4 |
| Field-induced strain | 27 ppm, see Figure 3-22 |

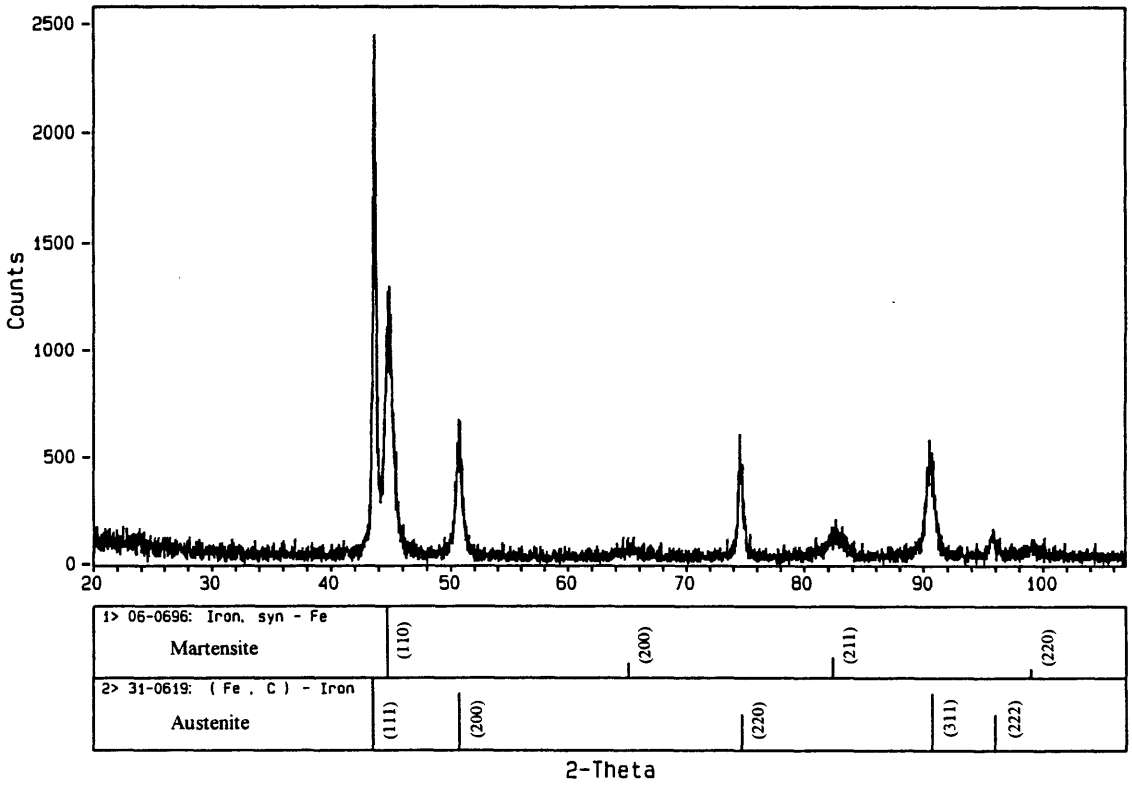


**Figure 4-4 X-ray diffraction of homogenized S1 followed by quenching in liquid nitrogen.**

## 4.8 Development of Fe-Ni-Co-Ti-based MSM alloys

Although the specimen with thin-plate martensite did not show any significant field-induced strain, we should start the development of Fe-Ni-Co-Ti-based MSM materials from this specimen, because thin-plate martensite has the potential to show MSM effect. The route to the development of Fe-Ni-Co-Ti-based MSM materials is discussed in three steps:

1) Observation of clear evidence of MSM effect

The apparent evidence of MSM effect has not yet been observed in Fe-Ni-Co-Ti. Therefore, the first step must be to confirm the MSM effect in this system. The reason why no significant field-induced strain was observed is likely the fact that only polycrystalline specimens were selected. Some degree of crystallographic texture in materials is required for MSM effects in order that strains in different grains do not cancel. One option is to perform MSM tests on single-crystals since large field-induced strains were observed in a single-crystal of $Ni_2MnGa$ [5, 8] and the result in a single crystal should give the maximum limit of the performance of the alloys.

Another option is a texturing of polycrystalline materials. Though a textured material still possesses a polycrystalline form, the field-induced strains of each grain may not cancel each other if a texture is present. Furuya found in 1998 that a rapidly solidified Fe-Pd(29.6 at%) showed field-induced strain of 0.17 % with a columnar-crystal structure [30]; this is a notable discovery which demonstrated that even a polycrystalline material can exhibit a significant field-induced strain with a texture. Cold working, such as rolling and torsion, also appear to be effective at introducing a strong texture. Moreover, stress-induced martensite can be expected if the material is austenitic before cold working. As

Murray et al. reported [7], stress-induced martensite has two advantages: preferentially aligned texture due to applied stress and extension of applicable temperature range beyond martensite start temperature ($T_{Ms}$). Therefore, a texturing by rapid solidification and cold working is attractive for MSM materials.

2) Increase of field-induced strain

Once a MSM effect is observed in this system, then the field-induced strain should be increased, assuming that the Fe-Ni-Co-Ti alloys have high enough hardness to generate the desired large field-induced force. One way is to accelerate the effect of a texture. Another way is that; based on O'Handley's model of the MSM effect as discussed in Section 4.5 [19], large saturation magnetization ($M_s$), small stiffness ($C$), and small transformation strain ($e_0$) are favorable for large field-induced strain at a given magnetic field. Stiffness may not change so much with alloying since Fe, Ni, and Co have almost the same elastic moduli of 210 GPa [31], assuming that stiffness is represented by elastic modulus. $M_s$ can be changed depending on the chemical compositions (Figure 3-16). Finally, the variation of $e_0$ should be examined to explore the effect of $e_0$.

3) Increase of operating temperature

In addition to the increase of the amount of field-induced strain, the operating temperature should be increased for practical applications. As discussed in Section 4.2, it can be achieved by the increase of the width of thermal hysteresis and by the increase of martensite start temperature, though it is limited by the formation of lenticular martensite.

# 5 Conclusion

This study is the first exploration of the possibility of developing magnetic shape-memory (MSM) materials based on Fe-Ni-Co-Ti alloys. The effects of chemical composition (Co/Ni ratio) and ausaging on microstructure and magnetic shape-memory response were studied in three ingots having different Co/Ni ratio and ausaging conditions. These ingots were hot rolled, homogenized, water quenched, and ausaged. The microstructures observed varied with chemical composition; while the lower Co/Ni alloys S1 and S2 showed austenite at room temperature without aging, the high Co/Ni alloy S3 showed martensite even at room temperature. Also, ausaging altered the microstructure and was effective in promoting the formation of martensite at room temperature, by raising the martensite start temperatures. Therefore, the proper choice of chemical composition and ausaging enables the formation of martensite at or above room temperature in these alloys.

The martensite morphology also varied with chemical composition and aging conditions, and most of the martensite observed in this research was lenticular or a mixture of lenticular and thin-plate morphology. Only homogenized S1 followed by quenching in liquid nitrogen showed typical thin-plate morphology. Although the martensite start temperature of homogenized S1 was low (203 K), thin-plate martensite still existed at room temperature after quenching in liquid nitrogen, due to the large thermal hysteresis of the austenite-martensite transformation in these alloys. This thin-plate martensite was fully twinned with no midrib. Since a twinned substructure is

required for MSM effect, lenticular martensite was not of particular interest in this study. Therefore, it can be concluded that the martensite start temperature ($T_{Ms}$) should be increased only to the extent that thin-plate morphology can be maintained.

Chemical composition and ausaging also had significant effects on mechanical hardness and saturation magnetization ($M_s$). Ausaging increased the hardness dramatically, possibly due to precipitation hardening of $(Fe,Ni,Co)_3Ti$, and increases in Co/Ni ratio accelerated the ausaging kinetics. High hardness is favorable for obtaining thin-plate martensite because slip becomes difficult in austenite at martensite-austenite interfaces with high hardness. Ausaging also increased $M_s$ through structural change, that is, austenite to martensite. While austenite showed $M_s$ less than 130 emu/g, martensite showed $M_s$ more than 140 emu/g, though the $M_s$ of martensite was relatively insensitive to the aging conditions. Higher Co/Ni ratio resulted in higher $M_s$, as expected. Since the ratio of stiffness (elastic modulus) and $M_s$ of Fe-Ni-Co-Ti is similar to that in $Ni_2MnGa$, it can be expected that Fe-Ni-Co-Ti has the potential to show the same order of strains as $Ni_2MnGa$, if the magnitude of transformation strain is the same in both materials.

Regardless of chemical composition and heat treatments, Curie temperatures of Fe-Ni-Co-Ti alloys studied were more than 473 K, and measurable tetragonality and texture due to hot rolling were not detected in X-ray diffraction.

Thin-plate martensite (homogenized S1 after quenching in liquid nitrogen) exhibited a significant conventional shape-memory effect, while lenticular martensite (homogenized S3) showed limited shape recovery; therefore, it is confirmed that thin-plate martensite has the potential for a shape reversibility.

Even in specimens of Fe-Ni-Co-Ti alloys that showed conventional shape memory behavior, no significant field-induced strains were observed. This result is thought to be due to the random grain orientation in the polycrystalline materials; namely the strains of each grains canceled each other, although each grain may show some field-induced deformation.

# 6 Bibliography


1 K.Ullakko, J. Mtls. Eng. Performance 5, 405 (1996).

2 K.Ullakko, International Conference on Intelligent Materials and Third European Conference on Smart Structures and Materials 1996 (ed. P.F.Gobin and J.Tatibouet), Proc. SPIE 2779, 505 (1996).

3 K.Ullakko, P.G.Yakovenko, and V.G.Gavriljuk, Proc. SPIE 2715, 42 (1996).

4 R.E.Reed-Hill and R.Abbaschian, Physical Metallurgy Principles, PWS Publishing Company, Boston (1994).

5 K.Ullakko, J.K.Huang, C.Kantner, R.C.O'Handley, and V.V.Kokorin, Appl. Phys. Lett. 69, 1966 (1996).

6 K.Ullakko, J.K.Huang, V.V.Kokorin, and R.C.O'Handley, Scr. Metall. Mater. 36, 1133 (1997).

7 S.J.Murray, M.Farinelli, C.Kantner, J.K.Huang, S.M.Allen, and R.C.O'Handley, J. Appl. Phys. 83, in press (1998).

8 R.D.James and M.Wuttig, Phil. Mag. A 77, 1273 (1998).

9 T.Maki, K.Kobayashi, and I.Tamura, Proc. of Int. Conf. On Martensitic Transformations (ICOMAT-82), J. Phys. Colloq. 43, C4-541 (1982).

10 T.Maki, S.Furutani, and I.Tamura, ISIJ International 29, 438 (1989).

11 T.Maki, K.Kobayashi, M.Minato, and I.Tamura, Scr. Metall. 18, 1105 (1984).

12 H.Kloβ, Z. Metallkd. 58, 372 (1996).

13 L.Jian, C.C.Chou, and C.M.Waymen, Materials Chemistry and Physics 34, 14 (1993).

14 T.Kikuchi and S.Kajiwara, Mater. Trans. JIM 34, 907 (1993).

15 N.Jost, Journal de Physique IV C4-445 (1991).

16 G.Kubla and E.Hornbogen, Journal de Physique IV C8-475 (1995).

17 R.M.Bozorth, Ferromagnetism, IEEE PRESS, New York (1993).

18 P.Villars, A.Prince, and H.Okamoto, Handbook of Ternary Phase Diagrams vol.7, ASM international (1995).

19 R.C.O'Handley, J. Appl. Phys. 83, 3236 (1998).

20 O.Johari and G.Thomas, Acta Metall. 12, 1211 (1965).

21 T.Maki, S.Shimooka, S.Fujiwara, and I.Tamura, Trans. JIM 16, 35 (1975).

22 K.Shimizu and C.M.Wayman, Acta Metall. 14, 1390 (1966).

23 S.K.Das and G.Thomas, Metall. Trans. 1, 325 (1970).

24 Z.Nishiyama, Martensitic Transformation, Academic Press, New York (1978).

25 V.V.Kokorin, L.P.Gun'ko, and O.M.Shevchenko, Physics of Met. and Metallogr. 74, 502 (1992).

26 P.Hassen, Phase Transformation in Materials, VCH, Weinheim (1991).

27 E.R.Petty, Martensite Fundamentals and Technology, Longman, London (1970).

28 J.D.Verhoeven, Fundamentals of Physical Metallurgy, John Wiley & Sons, New York (1975).

29 M.Marioni, (unpublished).

30 Y.Furuya, Abstract booklet of the ICAT 24 Smart Actuator symposium (April 20-21, 1998, Penn State University, PS, USA) 6 (1998).
31 N.E.Dowling, Mechanical Behavior of Materials, Prentice-Hall, Englewood Cliffs (1993).